

Sulphur and zinc abundances in Galactic halo stars revisited ^{*,**}

P.E. Nissen¹, C. Akerman², M. Asplund³, D. Fabbian³, F. Kerber⁴, H.U. Käuff⁴, and M. Pettini²

¹ Department of Physics and Astronomy, University of Aarhus, DK-8000 Aarhus C, Denmark. e-mail: pen@phys.au.dk

² Institute of Astronomy, University of Cambridge, Madingley Road, Cambridge, CB3 0HA, UK.

³ Research School of Astronomy and Astrophysics, Australian National University, Cotter Road, Weston, ACT 2611, Australia.

⁴ European Southern Observatory, Karl-Schwarzschild-Str. 2, D-85748 Garching, Germany.

Received 23 February 2007 / Accepted 2 April 2007

ABSTRACT

Aims. Based on a new set of sulphur abundances in very metal-poor stars and an improved analysis of previous data, we aim at resolving current discrepancies on the trend of S/Fe vs. Fe/H and thereby gain better insight into the nucleosynthesis of sulphur. The trends of Zn/Fe and S/Zn will also be studied.

Methods. High resolution VLT/UVES spectra of 40 main-sequence stars with $-3.3 < [\text{Fe}/\text{H}] < -1.0$ are used to derive S abundances from the weak $\lambda 8694.6$ S I line and the stronger $\lambda \lambda 9212.9, 9237.5$ pair of S I lines. For one star, the S abundance is also derived from the S I triplet at $1.046 \mu\text{m}$ recently observed with the VLT infrared echelle spectrograph CRIRES. Fe and Zn abundances are derived from lines in the blue part of the UVES spectra, and effective temperatures are obtained from the profile of the H β line.

Results. Comparison of sulphur abundances from the weak and strong S I lines provides important constraints on non-LTE effects. The high sulphur abundances reported by others for some metal-poor stars are not confirmed; instead, when taking non-LTE corrections into account, the Galactic halo stars distribute around a plateau at $[\text{S}/\text{Fe}] \sim +0.2$ dex with a scatter of 0.07 dex only. $[\text{Zn}/\text{Fe}]$ is close to zero for metallicities in the range $-2.0 < [\text{Fe}/\text{H}] < -1.0$ but increases to a level of $[\text{Zn}/\text{Fe}] \sim +0.1$ to $+0.2$ dex in the range $-2.7 < [\text{Fe}/\text{H}] < -2.0$. At still lower metallicities $[\text{Zn}/\text{Fe}]$ rises steeply to a value of $[\text{Zn}/\text{Fe}] \sim +0.5$ dex at $[\text{Fe}/\text{H}] = -3.2$.

Conclusions. The trend of S/Fe vs. Fe/H corresponds to the trends of Mg/Fe, Si/Fe, and Ca/Fe and indicates that sulphur in Galactic halo stars has been made by α -capture processes in massive SNe. The observed scatter in S/Fe is much smaller than predicted from current stochastic models of the chemical evolution of the early Galaxy, suggesting that either the models or the calculated yields of massive SNe should be revised. We also examine the behaviour of S/Zn and find that departures from the solar ratio are significantly reduced at all metallicities if non-LTE corrections to the abundances of these two elements are adopted. This effect, if confirmed, would reduce the usefulness of the S/Zn ratio as a diagnostic of past star-formation activity, but would bring closer together the values measured in damped Lyman-alpha systems and in Galactic stars.

Key words. Stars: abundances – Stars: atmospheres – Galaxy: halo – Galaxies: abundances – Galaxies: high-redshift

1. Introduction

Despite several recent papers on sulphur abundances in Galactic stars, there is still no agreement on the trend of $[\text{S}/\text{Fe}]$ vs. $[\text{Fe}/\text{H}]$ for halo stars. Some studies (Ryde & Lambert 2004, Nissen et al. 2004) indicate that $[\text{S}/\text{Fe}]$ is approximately constant at a level of $+0.3$ dex in the metallicity range $-3 < [\text{Fe}/\text{H}] < -1$. Such a plateau-like overabundance of S with respect to Fe is also predicted from Galactic chemical evolution models with Type II SNe as the dominant source of element production up to $[\text{Fe}/\text{H}] \sim -1$ (Chiappini et al. 1999, Goswami & Prantzos 2000); the decline of $[\text{S}/\text{Fe}]$ for galactic disk stars (Chen et al. 2002, Ryde 2006) is then due to the release of iron from Type Ia SNe at $[\text{Fe}/\text{H}] > -1$.

Other investigations point, however, to an increasing trend of $[\text{S}/\text{Fe}]$ towards lower metallicities (Israelian & Rebolo 2001; Takada-Hidai et al. 2002) with $[\text{S}/\text{Fe}]$ reportedly reaching as high as $+0.8$ dex at $[\text{Fe}/\text{H}] \sim -2$. As discussed by Israelian & Rebolo, such high values of $[\text{S}/\text{Fe}]$ may be explained if SNe with very large explosion energies of $E = (10 - 100) \times 10^{51}$ ergs (so-called hypernovae) make a substantial contribution to the nucleosynthesis of elements in the early Galaxy (Nakamura et al. 2001). An alternative explanation of an increasing trend of $[\text{S}/\text{Fe}]$ towards lower metallicities has been proposed by Ramaty et al. (2000): assuming a short mixing time (~ 1 Myr) for supernovae-synthesized volatile elements like oxygen and sulphur and a longer mixing time (~ 30 Myr) for refractory elements like Fe, high values of $[\text{O}/\text{Fe}]$ and $[\text{S}/\text{Fe}]$ are expected in the early Galaxy.

In a recent paper by Caffau et al. (2005), more puzzling data on $[\text{S}/\text{Fe}]$ in halo stars have been obtained. Both high $[\text{S}/\text{Fe}] \sim +0.8$ dex and low $[\text{S}/\text{Fe}] \sim +0.3$ dex are found in the metallicity range $-2.2 < [\text{Fe}/\text{H}] < -1.0$ (see Fig. 10 of Caffau et al.), suggesting a dichotomy of $[\text{S}/\text{Fe}]$. If real, this

* Based on observations collected at the European Southern Observatory at Paranal, Chile (programmes No. 67.D-0106, 73.D-0024 and CRIRES science verification program 60.A-9072)

** Table 1 and Appendices A, B, and C are only available in electronic form at <http://www.aanda.org>

points to a very complicated chemical evolution of sulphur in the early Galaxy.

Additional problems have been revealed by Takeda et al. (2005), who find that S abundances derived from the weak $\lambda 8694.6$ Si I line are systematically higher than S abundances derived from the stronger $\lambda\lambda 9212.9, 9237.5$ pair of lines when their new non-LTE corrections are applied.

The uncertainty about the trend of $[S/Fe]$ calls for further studies of sulphur abundances in halo stars. In this paper we present new sulphur abundances for 12 halo stars with $-3.3 < [Fe/H] < -1.9$ based on high-quality, near-IR spectra obtained with the VLT/UVES spectrograph. We have also re-analyzed UVES spectra of 28 stars with $[Fe/H] < -1$ from Nissen et al. (2004, hereafter Paper I) determining T_{eff} from the $H\beta$ line in the same way as for the new stars and improving the derivation of S abundances from the $\lambda\lambda 9212.9, 9237.5$ lines by taking into account the opacity contribution from the wings of the Paschen-zeta hydrogen line at 9229 \AA . In addition, possible non-LTE effects are investigated by comparing S abundances obtained from the weak Si I line at 8694.6 \AA with data from the $\lambda\lambda 9212.9, 9237.5$ Si I lines.

We have also derived zinc abundances from the $\lambda\lambda 4722.2, 4810.5$ Zn I lines. Both S and Zn are among the few elements which are not readily depleted onto dust in the interstellar medium of the Milky Way and are present in the gas-phase in near-solar proportions. For this reason, they are key to studies of metal enrichment in distant galaxies, particularly those detected as damped Lyman-alpha systems (DLAs) in the spectra of high redshift QSOs. Assuming that sulphur behaves like other α -capture elements and that Zn follows Fe, the S/Zn ratio may be used to date the star formation process in DLAs (Wolfe et al. 2005). A clarification of the trends of both S and Zn for Galactic stars is important to test if these assumptions are correct.

2. Observations and data reduction

The 12 new programme stars were selected from the list of very metal-poor turnoff stars in Ryan et al. (1999) and observed with the VLT/UVES spectrograph (Dekker et al. 2000) in service mode during ESO period 73 (April - September, 2004). In addition to the programme stars, a fast-rotating bright early-type B star (either HR 5488 or HR 6788) was observed on each night in order to be able to remove telluric H_2O lines in the $9212 - 9238 \text{ \AA}$ region.

The UVES setup was the same as described in Paper I except that no image slicer was applied when imaging the star onto the 0.7 arcsec wide entrance slit. Briefly, we mention that the dichroic mode of UVES was used to cover the spectral region $3750 - 5000 \text{ \AA}$ in the blue arm and $6700 - 10500 \text{ \AA}$ in the red arm, in both cases with a spectral resolving power of $\lambda/\Delta\lambda \simeq 60\,000$. The blue region contains a number of Fe II lines suitable for determining the iron abundance, and two Zn I lines. In the red region we find the weak $\lambda 8694.6$ Si I line as well as the stronger Si I lines at 9212.9 and 9237.5 \AA . Typical S/N ratios are 300 in the blue spectral region, 250–300 at the $\lambda 8694.6$ Si I line, and 150–200 in the $9212 - 9238 \text{ \AA}$ region.

The spectra were reduced by using standard IRAF routines for order definition, background subtraction, flat-field correction, order extraction with sky subtraction and wavelength calibration. Continuum fitting was performed with

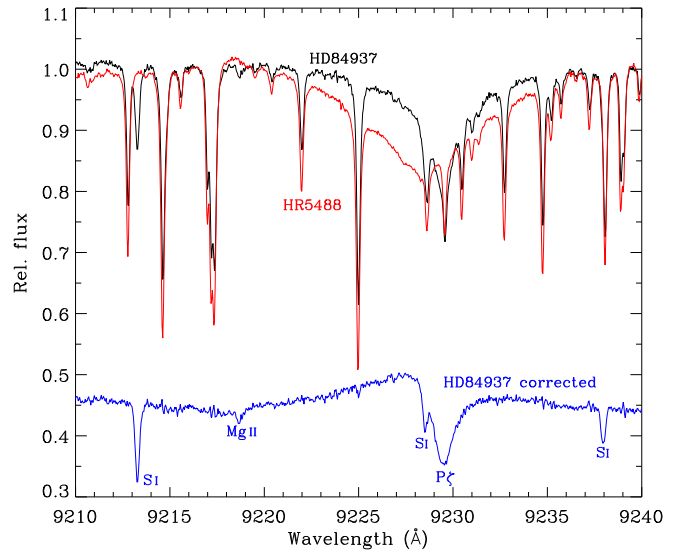


Fig. 1. The VLT/UVES spectrum of HD 84937 in the spectral region $9210 - 9240 \text{ \AA}$ overlaid with the B2III spectrum of HR 5488. Below is the spectrum of HD 84937 (shifted ~ 0.5 units in relative flux) after removal of the telluric lines using the IRAF task `telluric` to divide with a scaled version of the spectrum of HR 5488.

the IRAF task `continuum` using spline functions with a scale of a few \AA . Since many continuum windows are available for these metal-poor stars, even in the blue part of the spectrum, this method works well.

The quality of the 2004 spectra is about the same as shown in Fig. 2 of Paper I. As an additional illustration of the removal of telluric lines, we show the spectrum of HD 84937 in Fig. 1. This bright star was observed with particularly high S/N. As seen from the figure, the $\lambda 9237.5$ Si I line is completely overlapped by a telluric line, but after division with the scaled B-type spectrum of HR 5488, the line emerges very clearly. Due to the radial velocity difference of the two stars, the P ζ H I line at 9229 \AA is seen as a broad feature in ‘emission’ from HR 5488 overlaid with a narrower absorption line from HD 84937. The wings of the P ζ line are lost and therefore the equivalent widths of the Si I lines can only be measured relative to the local continuum. Hence, when using their equivalent widths to derive S abundances, the opacity contribution from the P ζ line should be taken into account.

Interference fringing is another problem in the near-IR part of the spectrum. The fringes on the UVES MIT CCD have an amplitude of 20 - 40 % at 9000 \AA . After flat-fielding, residual fringes at a level of $\pm 0.5\%$ remain as seen from Fig. 2. As discussed by Korn & Ryde (2005), this makes it difficult to determine precise S abundances of halo stars from the weak $\lambda 8694.6$ Si I line. B-type stars may, however, also be used to correct for the residual fringing as illustrated in Fig. 2. After division by the spectrum of HR 5488, the spectrum of HD 84937 has a S/N ~ 500 . Without such a correction, the error of the S abundance derived from the $\lambda 8694.6$ line can be large, especially for stars with $[Fe/H] < -2$.

Equivalent widths of S, Fe and Zn lines were measured by Gaussian fitting or direct integration if the fit was poor and are given in Table A.1 for the 12 stars observed in 2004.

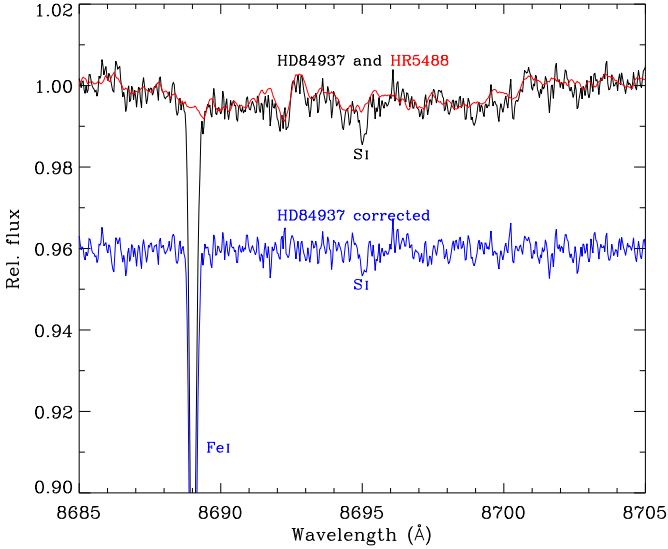


Fig. 2. The VLT/UVES spectrum of HD 84937 in the spectral region 8685 – 8705 Å overlaid with the B2III spectrum of HR 5488. Below is the spectrum of HD 84937 (shifted down 0.04 units in relative flux) after division with the spectrum of HR 5488.

The corresponding table for the Paper I stars is available at the CDS¹.

3. Model atmospheres and stellar parameters

The determination of the effective temperature (T_{eff}) as well as the abundances of S, Fe and Zn is based on α -element enhanced ($[\alpha/\text{Fe}] = +0.4$, $\alpha = \text{O, Ne, Mg, Si, S, Ca, and Ti}$) 1D model atmospheres computed with the Uppsala MARCS code. Updated continuous opacities (Asplund et al. 1997) including UV line blanketing are used. LTE is assumed both in constructing the models and in deriving T_{eff} and the abundances. Convection is treated in the approximation of Henyey et al. (1965) with a mixing-length parameter of $\alpha_{\text{MLT}} = l/H_p = 1.5$, and a temperature distribution in the convective elements determined by the diffusion equation (parameter $y = 3/4\pi^2 = 0.076$). The reader is referred to Ludwig et al. (1999) for a summary of the parameters used in different versions of the mixing length theory.

3.1. Effective temperature

Instead of deriving T_{eff} from the $(b-y)$ and $(V-K)$ colour indices as in Paper I, we decided to use the profile of the $\text{H}\beta$ line in the blue part of the UVES spectra. The advantage is that the $\text{H}\beta$ -based T_{eff} is not affected by possible errors in the interstellar reddening; in general the new stars are more distant than the stars in Paper I and hence potentially more affected by interstellar absorption.

The $\text{H}\beta$ line is well centered in an echelle order having a width of approximately 80 Å. After flat-fielding, the continua of the two adjacent echelle orders were fitted by low order spline functions and the continuum of the $\text{H}\beta$ order was determined by interpolation between these functions in pixel space. The $\text{H}\beta$ echelle order is not wide enough

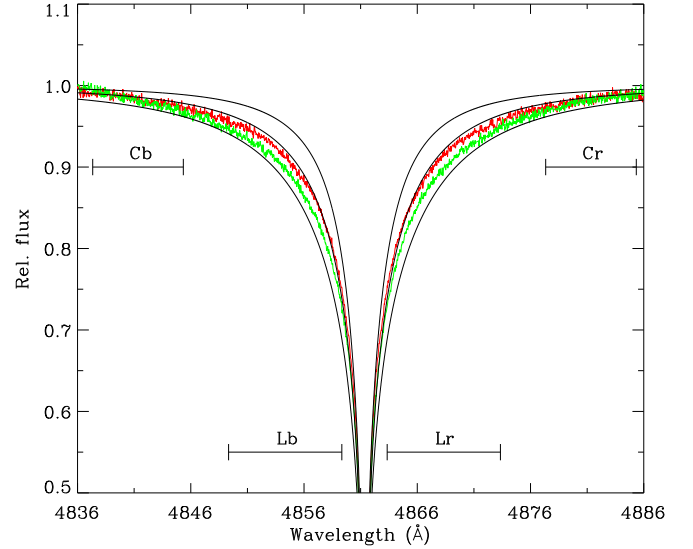


Fig. 3. Observed $\text{H}\beta$ profiles in the spectra of CD $-24^\circ 17504$ ($T_{\text{eff}} = 6340$ K, upper jagged line) and LP 815-43 ($T_{\text{eff}} = 6480$ K, lower jagged line) compared to synthetic profiles (thin lines) computed for model atmospheres with $\log g = 4.3$, $[\text{Fe}/\text{H}] = -2.8$ and $T_{\text{eff}} = 6000, 6300, 6600$ K, respectively. An index, $\beta(\text{UVES})$, measuring the strength of the $\text{H}\beta$ line is defined from the total flux in the C bands relative to the total flux in the L bands (see Appendix B).

to reach the true continuum, but the method allows one to use the inner ± 30 Å of the profile to derive T_{eff} from a comparison with synthetic $\text{H}\beta$ profiles for a grid of model atmospheres. In addition to the 12 new stars, T_{eff} was also re-determined in this way for stars from Paper I.

To illustrate this method, Fig. 3 shows the $\text{H}\beta$ profiles in the spectra of two stars compared to synthetic profiles calculated as described in Barklem et al. (2002) using Stark broadening from Stehlé & Hutcheon (1999) and self-broadening from Barklem et al. (2000a). A few metallic absorption lines have been removed by interpolating the $\text{H}\beta$ profile across these lines. An index, $\beta(\text{UVES})$, defined as the ratio of the total flux in the two C-bands to the total flux in the two L bands is used to determine T_{eff} (see Appendix B). Hence, we are not using the position of the true continuum in determining T_{eff} . The center of the $\text{H}\beta$ line is also avoided, because the fit between theoretical and observed profiles is poor around the line center due to non-LTE effects (Przybilla & Butler 2004).

For stars with $[\text{Fe}/\text{H}] > -1$, the metal lines in the $\text{H}\beta$ line are so strong that the removal of these lines by interpolation of the profile across the lines is unreliable. Hence, six stars with $[\text{Fe}/\text{H}] > -1$ from Paper I are not included in the present paper.

The symmetric appearance of the observed profiles shows that the procedure of rectifying the $\text{H}\beta$ echelle order has worked well. In fact, the difference between T_{eff} determined from the left and the right part of the $\text{H}\beta$ profile never exceeded 30 K. The internal stability of the method is also very good; the effective temperatures determined for a given star observed on different nights agreed within ± 20 K. Another advantage is that the profile of the $\text{H}\beta$ line varies very little with gravity and metallicity. Hence, the errors in these parameters have only a small effect on the derived T_{eff} . For a group of stars with similar atmospheric

¹ <http://cdsweb.u-strasbg.fr/cgi-bin/qcat?/A+A/415/993>

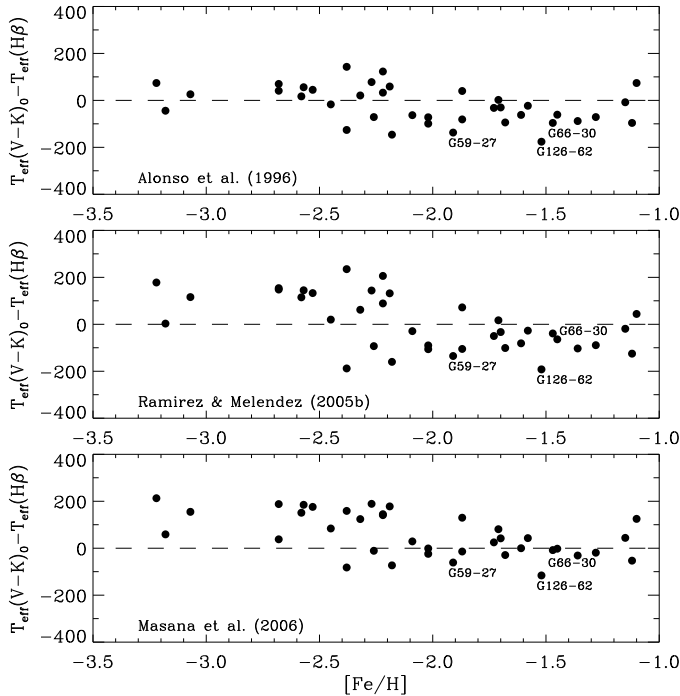


Fig. 4. The difference of effective temperatures derived from $(V-K)_0$ and $H\beta$ using three different calibrations of $(V-K)_0$. The comparison includes only 38 stars; LP 651-4 falls outside the range in $(V-K)_0$ where the calibrations are valid, and CD $-71^\circ 1234$ is missing Strömgren photometry; hence, its interstellar reddening excess, $E(V-K)$, could not be derived. Three stars known to be single-lined spectroscopic binaries are marked.

parameters, like metal-poor turnoff stars, one might therefore expect that differential values of T_{eff} can be determined with a precision of about ± 30 K from the $H\beta$ profile.

The systematic error of T_{eff} is, however, larger. The fit between the theoretical and observed profiles is not perfect in the central region of the $H\beta$ line, and the estimated value of T_{eff} therefore depends to some extent on where the L-bands of the $H\beta$ index are placed. The temperature structure of the model atmospheres also plays a role. If the mixing-length parameter is decreased from $l/H_p = 1.5$ to 1.0, the derived T_{eff} changes by about -25 K for metal-poor stars at the turnoff ($T_{\text{eff}} \sim 6400$ K) and about -60 K for cooler stars ($T_{\text{eff}} \sim 5800$ K).

The derived effective temperatures are given in Table 1. Ten of the stars are in common with Asplund et al. (2006), who determined T_{eff} from the $H\alpha$ profile in independent UVES spectra. The average difference, $T_{\text{eff}}(H\beta) - T_{\text{eff}}(H\alpha)$ is 64 K with a rms scatter of the deviation of ± 28 K. This small scatter confirms that precise differential values of T_{eff} can be determined from $H\alpha$ and $H\beta$ for stars with similar atmospheric parameters, but the systematic difference indicates that the absolute values of T_{eff} are more uncertain. Interestingly, the systematic difference of $T_{\text{eff}}(H\beta)$ and $T_{\text{eff}}(H\alpha)$ vanishes if the mixing-length parameter is decreased to $l/H_p = 0.5$. The same conclusion was reached by Fuhrmann et al. (1993) for a set of Kurucz model atmospheres with the convective structure parameter $y = 0.5$. Given that Barklem et al. (2002) were not able to obtain a satisfactory fit to the $H\alpha$ and $H\beta$ line profiles in the solar spectrum for any combination of the

convection parameters l/H_p and y , it seems, however, premature to change these parameters from the standard values of the MARCS models. Clearly, the model atmospheres and/or the line broadening theory need to be improved. Although it is often argued in the literature that the wings of Balmer lines are formed in LTE for late-type stars, very recent work suggests that this may in fact not necessarily be true (Barklem 2007). Unfortunately, the degree of departures from LTE depends critically on still poorly known inelastic collisions with other neutral H atoms. Some existing atomic calculations imply LTE while others yield significant non-LTE effects. A full 3D non-LTE analysis of Balmer line profiles in cool stars with improved collisional data is urgently needed to resolve this potentially significant systematic error.

The problem of systematic errors in the effective temperatures of metal-poor stars is also evident when comparing $T_{\text{eff}}(H\beta)$ with effective temperatures derived from the $(V-K)_0$ index using three different colour- T_{eff} calibrations (see Fig. 4). Here, the V magnitude was taken from Strömgren photometry (see Table B.1), and K from the 2MASS catalogue (Skrutski et al. 2006). Correction for reddening was applied according to the relation $E(V-K) = 3.8 E(b-y)$ (Savage & Mathis 1979), where $E(b-y)$ is derived as described in Appendix B.

The $(V-K)_0$ calibrations of Ramírez & Meléndez (2005b) and Masana et al. (2006) refer directly to the 2MASS K_s magnitude system, whereas the Alonso et al. (1996) calibration refer to the original Johnson (1966) K_J system. Hence, before applying the Alonso et al. calibration, we converted K_s to K_J using equations in Alonso et al. (1994) relating K_J to K_{CIT} (Elias et al. 1982) and the transformation from K_s to K_{CIT} derived by Cutri et al. (2006). These transformations all contain a small $(J-K)$ colour term, but since our sample of stars are confined to a narrow range in $J-K$, we get in a good approximation $(V-K_J) \simeq (V-K_s) - 0.035$ for metal-poor stars in the turnoff region. If this transformation had not been applied, the effective temperatures derived from $(V-K)_0$ with the Alonso et al. calibration would have been about 65 K lower.

As seen from Fig. 4, there is good agreement between T_{eff} from $H\beta$ and from $(V-K)_0$ when using the Alonso et al. (1996) calibration. Excluding the three known binary stars, the mean difference, $T_{\text{eff}}(V-K)_0 - T_{\text{eff}}(H\beta)$ is -11 ± 72 K. The scatter agrees well with the error of $T_{\text{eff}}(V-K)_0$ expected from errors in the reddening correction. Still, there is a tendency for the residuals to increase with decreasing $[Fe/H]$. This tendency is even more pronounced for the $(V-K)_0$ calibrations of Ramírez & Meléndez (2005b) and Masana et al. (2006). When using the $(V-K)_0$ calibration of Ramírez & Meléndez, stars with $[Fe/H] > -2.0$ have a mean deviation $T_{\text{eff}}(V-K)_0 - T_{\text{eff}}(H\beta)$ of about -50 K, whereas stars with $[Fe/H] < -2.5$ have a mean deviation of $+124$ K. Hence, our $H\beta$ -based effective temperatures do not confirm the hot T_{eff} scale of very metal-poor turnoff stars derived by Ramírez & Meléndez (2005a) from their application of the infrared flux method.

Four of the stars in Table 1 are known to be single-lined spectroscopic binaries, i.e. G 66-30 (Carney et al. 2001), G 126-62 and G 59-27 (Latham et al. 2002), and CD $-71^\circ 1234$ (Ryan et al. 1999). As discussed by Ramírez et al. (2006) in the case of G 126-62, these stars may have a cool companion that causes too low a value of T_{eff} to be derived from $(V-K)_0$. Indeed, G 126-62 and G 59-27 exhibit

Table 1. Derived stellar parameters and abundances of sulphur and zinc. LTE sulphur abundances are given for each of the three S I lines. The LTE Zn abundance is the average of the values derived from the $\lambda\lambda 4722.2, 4810.5$ Zn I lines. In calculating [S/Fe] and [Zn/Fe], solar abundances $\log \epsilon(\text{Fe})_{\odot} = 7.50$, $\log \epsilon(\text{S})_{\odot} = 7.20$ and $\log \epsilon(\text{Zn})_{\odot} = 4.60$ have been adopted. The non-LTE values of [S/Fe] and [Zn/Fe] are based on the non-LTE corrections calculated by Takeda et al. (2005) for a hydrogen collisional parameter $S_{\text{H}} = 1$.

ID	T_{eff} (K)	$\log g$ (cgs)	[Fe/H]	ξ_{turb} (km s^{-1})	$\log \epsilon(\text{S})_{\text{LTE}}$			[S/Fe]	[S/Fe]	$\log \epsilon(\text{Zn})$	[Zn/Fe]	[Zn/Fe]
					$\lambda 9212.9$	$\lambda 9237.5$	$\lambda 8694.6$	LTE	non-LTE	LTE	LTE	non-LTE
Paper I stars												
BD $-13^{\circ} 3442$	6366	3.99	-2.69	1.5	4.92	4.95		0.43	0.23	1.99	0.08	0.19
CD $-30^{\circ} 18140$	6272	4.12	-1.89	1.5	5.59	5.68	5.52	0.29	0.21	2.74	0.03	0.10
CD $-35^{\circ} 14849$	6294	4.26	-2.34	1.5	5.14	5.16		0.29	0.18	2.33	0.07	0.14
CD $-42^{\circ} 14278$	6085	4.39	-2.03	1.5	5.35	5.40		0.20	0.14	2.65	0.08	0.12
G 11-44	6178	4.35	-2.03	1.5	5.54	5.49		0.34	0.27	2.76	0.19	0.24
G 13-09	6343	4.01	-2.29	1.5	5.38			0.47	0.31	2.40	0.09	0.18
G 18-39	6093	4.19	-1.46	1.5	6.05	6.09	6.08	0.33	0.26	3.22	0.08	0.13
G 20-08	6194	4.29	-2.19	1.5	5.26	5.40		0.32	0.24	2.56	0.15	0.21
G 24-03	6084	4.23	-1.62	1.5	5.98	5.91	5.89	0.34	0.29	3.04	0.06	0.11
G 29-23	6194	4.04	-1.69	1.5	5.76	5.79	5.84	0.29	0.20	2.86	-0.05	0.02
G 53-41	5993	4.22	-1.29	1.3	6.18	6.16	6.19	0.27	0.20	3.33	0.02	0.06
G 64-12	6435	4.26	-3.24	1.5	4.41			0.45	0.19	1.77	0.41	0.52
G 64-37	6432	4.24	-3.08	1.5	4.45			0.33	0.10	1.96	0.44	0.55
G 66-30 ^{a)}	6470	4.29	-1.48	1.5	6.03	6.11	5.84	0.28	0.18	3.10	-0.02	0.05
G 126-62 ^{a)}	6224	4.11	-1.55	1.5	5.95	5.96	5.78	0.25	0.16	3.04	-0.01	0.05
G 186-26	6417	4.42	-2.54	1.5	4.85	4.85		0.19	0.07	2.25	0.19	0.26
HD 106038	6027	4.36	-1.37	1.2	6.28	6.22	6.29	0.43	0.38	3.37	0.14	0.18
HD 108177	6156	4.28	-1.71	1.5		5.86	5.78	0.33	0.30	2.96	0.07	0.12
HD 110621	6157	4.08	-1.59	1.5	6.03	5.92	5.74	0.29	0.21	3.02	0.01	0.07
HD 140283	5849	3.72	-2.38	1.5	5.07	5.06	5.17	0.28	0.20	2.30	0.08	0.14
HD 160617	6047	3.84	-1.75	1.5	5.81	5.80	5.85	0.37	0.28	2.82	-0.03	0.04
HD 179626	5881	4.02	-1.12	1.4	6.37		6.31 ^{b)}	0.26	0.17	3.48	0.00	0.04
HD 181743	6044	4.39	-1.87	1.5	5.62	5.62		0.29	0.23	2.81	0.08	0.12
HD 188031	6234	4.16	-1.72	1.5	5.76	5.75	5.78	0.28	0.21	2.91	0.03	0.09
HD 193901	5699	4.42	-1.10	1.2	6.29	6.30	6.34	0.21	0.17	3.38	-0.12	-0.10
HD 194598	6020	4.30	-1.15	1.4	6.26	6.30	6.20 ^{b)}	0.20	0.13	3.37	-0.08	-0.04
HD 215801	6071	3.83	-2.28	1.5	5.28	5.16		0.30	0.17	2.41	0.09	0.17
LP 815-43	6483	4.21	-2.71	1.5	4.87	4.81		0.35	0.17	2.17	0.28	0.38
New stars												
CD $-24^{\circ} 17504$	6338	4.32	-3.21	1.5	4.51			0.52	0.30	1.96	0.57	0.66
CD $-71^{\circ} 1234^{\text{a)}}$	6325	4.18	-2.38	1.5	5.13	5.19		0.34	0.22	2.34	0.12	0.20
CS 22943-095	6349	4.18	-2.24	1.5	5.36	5.33		0.38	0.26	2.49	0.13	0.20
G 04-37	6308	4.25	-2.45	1.5	5.05	4.98		0.26	0.15	2.29	0.14	0.21
G 48-29	6482	4.25	-2.60	1.5	4.94	5.03		0.39	0.23	2.13	0.13	0.23
G 59-27 ^{a)}	6272	4.23	-1.93	1.5	5.57	5.57		0.30	0.20	2.73	0.06	0.12
G 126-52	6396	4.20	-2.21	1.5	5.21			0.22	0.09	2.50	0.11	0.19
G 166-54	6407	4.28	-2.58	1.5	5.04	5.06		0.43	0.29	2.10	0.08	0.16
HD 84937	6357	4.07	-2.11	1.5	5.47	5.38	5.40	0.33	0.23	2.55	0.06	0.15
HD 338529	6373	4.03	-2.26	1.5	5.36	5.32		0.40	0.25	2.48	0.14	0.23
LP 635-14	6367	4.11	-2.39	1.5	5.12	5.07		0.29	0.14	2.36	0.15	0.24
LP 651-4	6371	4.20	-2.63	1.5	4.83			0.26	0.11	2.04	0.07	0.16

^{a)} Single-lined spectroscopic binary star.

^{b)} The weaker $\lambda 8694.0$ S I line is included in the determination of this S abundance.

some of the largest deviations in Fig. 4, whereas G 66-30 does not show a significant deviation. This star has an unusually high effective temperature ($T_{\text{eff}} = 6470$ K) for a halo star with $[\text{Fe}/\text{H}] = -1.48$, and is classified as a blue straggler by Carney et al. (2001).

3.2. Surface gravity

As in Paper I, the surface gravity is determined from the fundamental relation

$$\log \frac{g}{g_{\odot}} = \log \frac{\mathcal{M}}{\mathcal{M}_{\odot}} + 4 \log \frac{T_{\text{eff}}}{T_{\text{eff},\odot}} + 0.4(M_{\text{bol}} - M_{\text{bol},\odot}) \quad (1)$$

where \mathcal{M} is the mass of the star and M_{bol} the absolute bolometric magnitude.

The Strömgren indices ($b - y$), m_1 and c_1 were used to derive absolute visual magnitudes M_V (see Appendix B).

If the Hipparcos parallax (ESA 1997) of the star is available with an error $\sigma(\pi)/\pi < 0.3$, then M_V was also determined directly and averaged with the photometric value. The bolometric correction was adopted from Alonso et al. (1995) and the stellar mass derived by interpolating in the $M_V - \log T_{\text{eff}}$ diagram between the α -element enhanced evolutionary tracks of Vandenberg et al. (2000). As discussed in Paper I, the error of $\log g$ is estimated to be about ± 0.15 dex.

For one star, CD $-71^\circ 1234$, neither *wby*- β photometry nor the Hipparcos parallax is available. In this case, we estimated $\log g$ by requiring that the difference in the Fe abundance derived from Fe I and Fe II lines should equal the average difference between the two sets of Fe abundances for the other stars (see Sect. 4.1).

The derived values of T_{eff} and $\log g$ are mutually dependent and are also affected by $[\text{Fe}/\text{H}]$. Hence, the procedure of determining atmospheric parameters and Fe abundances was iterated until consistency was achieved. The final values obtained are given in Table 1.

4. Stellar abundances

Using MARCS model atmospheres with the parameters listed in Table 1, the Uppsala EQWIDTH and BSYN programs were used to compute equivalent widths of observed lines as a function of the corresponding element abundance. By interpolation to the observed equivalent width, the abundance of the element is then derived. A basic assumption is LTE, but the effect of possible departures from LTE will be discussed.

4.1. Iron

The Fe abundances are based on the Fe II lines listed in Table 2 of Paper I. The gf values of these lines were derived by an inverted abundance analysis of four ‘standard’ stars, for which iron abundances were adopted from Nissen et al. (2002). Hence, our $[\text{Fe}/\text{H}]$ scale is tied to that of Nissen et al., who used a set of very weak Fe II lines in the red spectral region to determine differential Fe abundances with respect to the Sun. The gf values agree very well with those recently derived by Melendéz et al. (2006) from Fe II radiative lifetime measurements of Schnabel et al. (2004) and branching ratios computed by R.L. Kurucz. The average difference of $\log gf$ (Melendéz et al. – Paper I) for the 19 Fe II lines is $+0.04$ dex with a scatter of ± 0.06 dex only.

Collisional line broadening was included in accordance with Barklem & Aspelund-Johansson (2005). For the large majority of stars, the Fe II lines are so weak that the derived metallicity is insensitive to possible errors in the van der Waals damping constant and also practically independent of the microturbulence parameter. Stars with $[\text{Fe}/\text{H}] < -1.5$ are assumed to have $\xi_{\text{turb}} = 1.5 \text{ km s}^{-1}$. For more metal-rich stars ξ_{turb} was determined by requesting that the derived $[\text{Fe}/\text{H}]$ value should be independent of equivalent width.

For all new stars, the Fe abundance was also determined from seven unblended Fe I lines selected to be of similar strengths as the Fe II lines. Wavelengths, gf -values (adopted from O’Brian et al. 1991) and measured equivalent widths are given in Table A.1. Collisional broadening data were adopted from Barklem et al. (2000b).

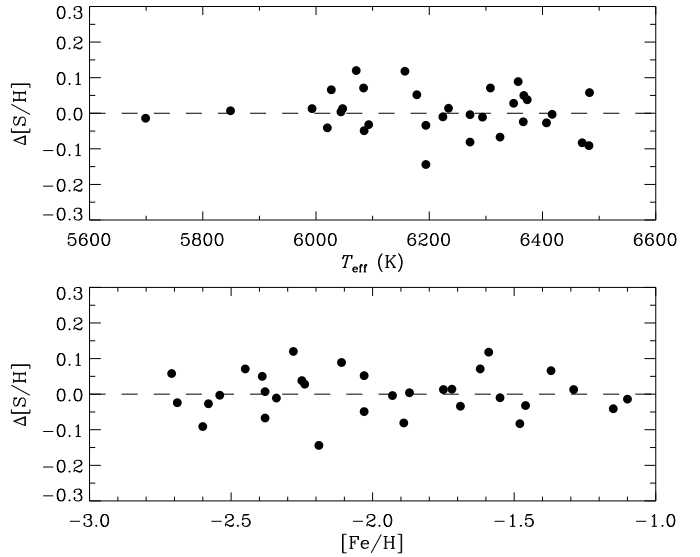


Fig. 5. The difference in S abundances derived from the $\lambda 9212.9$ and $\lambda 9237.5$ S I lines as a function of T_{eff} and $[\text{Fe}/\text{H}]$. The rms deviation between the two sets of abundances is ± 0.06 dex.

The average difference between Fe abundances derived from Fe II and Fe I lines is 0.14 dex with a rms deviation of ± 0.03 dex. This small scatter testifies to the high internal precision obtained. The systematically higher Fe abundance obtained from Fe II lines may be due to non-LTE effects on the Fe I lines (see discussion in Asplund 2005), although the scale of T_{eff} and/or the gf -values could also play a role. We note that the Fe II - Fe I differences are very similar to those estimated in Asplund et al. (2006). The $[\text{Fe}/\text{H}]$ values given in Table 1 are based on the Fe II lines, and refer to an adopted solar iron abundance of $\log \epsilon(\text{Fe})_{\odot} = 7.50$, which is close to the value inferred from weak Fe II lines in the solar spectrum using a MARCS model for the Sun (Nissen et al. 2002).

4.2. Sulphur

Sulphur abundances were derived from the observed equivalent widths of the high excitation S I lines at 8694.6, 9212.9 and 9237.5 Å. In two of the most metal-rich stars (HD 179626 and HD 194598), the $\lambda 8694.0$ S I line could also be detected, and hence its corresponding S abundance was averaged with that from the $\lambda 8694.6$ line. The atomic data for the lines are given in Table A.1. The gf -values (adopted from Coulomb approximation calculations of Lambert & Luck 1978) agree well with the experimental values of Bridges & Wiese (1967). Somewhat different gf -values have been calculated by Biéumont et al. (1993) but, as noted in Paper I, our adopted gf -values lead to a solar abundance $\log \epsilon(\text{S})_{\odot} = 7.20$, when the $\lambda \lambda 8694.0, 8694.6$ lines are analyzed with a MARCS model of the Sun. This is close to the meteoritic abundance of sulphur, $\log \epsilon(\text{S}) = 7.16 \pm 0.04$ (Asplund et al. 2005).

As mentioned in Sect 2, the equivalent widths of the S I lines at 9212.9 and 9237.5 Å were measured relative to the flux in the wings of the Paschen-zeta H I line at 9229 Å. In Paper I, the effect of Pζ was neglected, but here we include the opacity contribution from the wings when computing the equivalent widths. As in the case of Hβ, a version of the

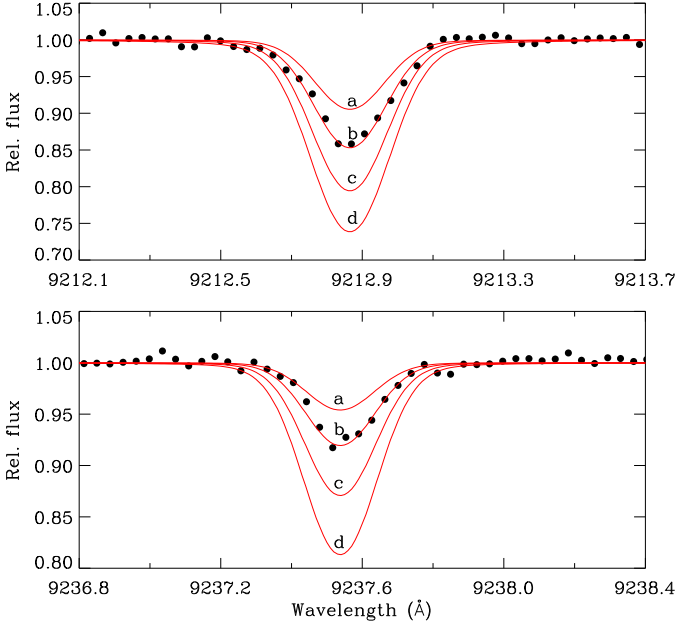


Fig. 6. UVES observations (dots) of the $\lambda\lambda 9212.9, 9237.5$ Si I lines in the spectrum of HD 181743. The four synthetic profiles marked by *a*, *b*, *c* and *d* refer to $\log \epsilon(\text{S}) = 5.33, 5.63, 5.93$ and 6.23 corresponding to $[\text{S}/\text{Fe}] = 0.0, 0.3, 0.6$ and 0.9 , respectively.

Uppsala BSYN program kindly supplied by P. Barklem was used in these calculations. The maximum effect of P ζ on the derived S abundances occurs for the hottest turnoff stars and amounts to an increase of $\log \epsilon(\text{S})$ by about 0.07 dex in the case of the 9237.5 \AA line and about 0.02 dex for the 9212.9 \AA line. After inclusion of the P ζ opacity, there is an excellent agreement between S abundances derived from the two lines with no significant trend of the deviation as a function of T_{eff} or $[\text{Fe}/\text{H}]$ (see Fig. 5), in contrast to the corresponding figure in Paper I, where a small but significant trend with T_{eff} was seen.

The sulphur abundances derived from the equivalent widths of the three Si I lines are given in Table 1 together with the average value of $[\text{S}/\text{Fe}]$. For some stars it was tested that a detailed synthesis of the observed profiles of the Si I lines yields practically the same abundances as the equivalent widths (see example in Fig. 6).

Table 1 includes three bright halo stars, HD 84937, HD 140283 and HD 181743, claimed by others to have very high sulphur abundances, $[\text{S}/\text{Fe}] \gtrsim +0.6$, whereas we find these stars to have $[\text{S}/\text{Fe}]$ around $+0.3$ dex. In trying to find the reason for this discrepancy, we briefly discuss these stars. Fig. 7 shows the spectrum synthesis of their Si I lines at 8694 \AA . The instrumental and stellar line broadening profile was approximated by a Gaussian with a FWHM of 8 km s^{-1} in the case of HD 84937 and 6 km s^{-1} for the other two stars. These values were derived from fitting the Fe I line at 8688.6 \AA .

4.2.1. HD 84937

From a KECK/HIRES spectrum of HD 84937, Takada-Hidai et al. (2002) measured the equivalent width of the $\lambda 8694.6$ Si I line to be $W_\lambda = 3.4 \text{ m\AA}$ and derived $\log \epsilon(\text{S}) = 5.7$ corresponding to $[\text{S}/\text{Fe}] = +0.6$. From our UVES spec-

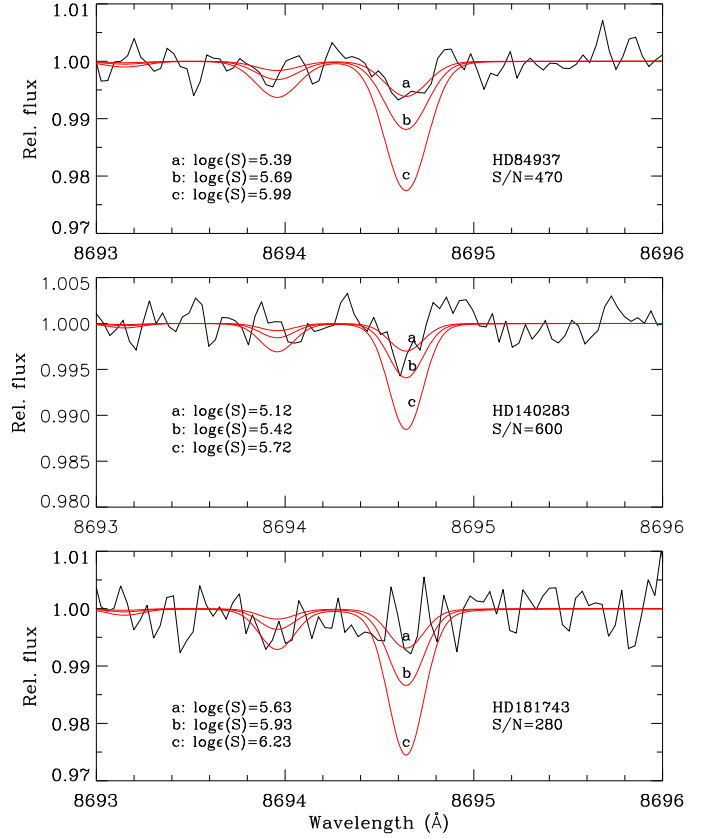


Fig. 7. UVES spectra (jagged line) of the region around the $\lambda 8694.6$ Si I line. For each star, the three synthetic profiles marked by *a*, *b* and *c* correspond to $[\text{S}/\text{Fe}] = 0.3, 0.6$ and 0.9 .

trum we measure $W_\lambda = 1.6 \pm 0.3 \text{ m\AA}$, where the quoted (1-sigma) error is estimated from the S/N of the spectrum and the uncertainty of the continuum setting. The correspondingly derived sulphur abundance is $\log \epsilon(\text{S}) = 5.40 \pm 0.08$. As shown in Fig. 7, this agrees well with the spectrum synthesis of the line; a value as high as $\log \epsilon(\text{S}) = 5.7$ is clearly excluded. Furthermore, we obtain $\log \epsilon(\text{S}) = 5.39$ and 5.48 from the $\lambda\lambda 9212.9, 9237.5$ Si I lines. Altogether, our sulphur abundance of HD 84937 is about a factor of two lower than the value found by Takada-Hidai et al. (2002).

4.2.2. HD 140283

Using the UVES Paranal Observatory Project (Bagnulo et al. 2003) spectrum of HD 140283, Takeda et al. (2005) derived $[\text{S}/\text{Fe}] \sim +1.0$ (corresponding to $\log \epsilon(\text{S}) \sim 5.8$) from the $\lambda 8694.6$ Si I line (see Fig. 7 in Takeda et al. 2005). As seen from our Fig. 7, we barely detect this line in our S/N ~ 600 spectrum of HD 140283; clearly, $\log \epsilon(\text{S})$ is much lower than 5.8 dex. From the measured equivalent width of the $\lambda 8694.6$ line, $W_\lambda = 0.7 \pm 0.3 \text{ m\AA}$, we get $\log \epsilon(\text{S}) = 5.17 \pm 0.20$ in good agreement with the result from the $\lambda\lambda 9212.9, 9237.5$ Si I lines, i.e. $\log \epsilon(\text{S}) = 5.07$ and 5.06 , respectively. Judging from Fig. 7 in Takeda et al. (2005), the UVES POP spectrum of HD 140283 is affected by residual fringing, which in this case apparently has led to a spurious enhancement of the $\lambda 8694.6$ Si I line, as also pointed out by Korn & Ryde (2005). Furthermore, it seems that

Takeda et al. have placed the continuum in the $\lambda 8694.6$ region too high. Using the same UVES POP spectrum with a more reasonable continuum, Takada-Hidai (2005) derived $\log \epsilon(\text{S}) = 5.53$ from the $\lambda 8694.6$ line. This is, however, still much higher than our value and also higher than the value of $\log \epsilon(\text{S}) = 5.18$, which they derive from the $\lambda 9237.5$ S I line.

4.2.3. HD 181743

For this star, Caffau et al. (2005) obtained $\log \epsilon(\text{S}) = 6.23$ and $[\text{S}/\text{Fe}] = +0.84$. The result is based on an apparently clear detection of the $\lambda 8694.6$ S I line in a UVES spectrum with $\text{S}/\text{N} = 180$ (P. Bonifacio, private communication). However, we cannot detect this line in our $\text{S}/\text{N} \sim 280$ spectrum as seen from Fig. 7, but estimate a 3-sigma upper limit of the equivalent width, $W_\lambda < 2 \text{ m}\text{\AA}$ corresponding to $\log \epsilon(\text{S}) < 5.8$. Caffau et al. did not use other S I lines for this star, whereas we derive $\log \epsilon(\text{S}) = 5.62$ from the $\lambda \lambda 9212.9, 9237.5$ lines. As seen from Fig. 6 the fit of the corresponding synthetic profiles to the observed lines is excellent.

We note that the large differences between sulphur abundances derived in the cited works and in the present paper cannot be explained in terms of different values of T_{eff} and $\log g$. In our view, it is more likely that the S abundances derived by others from the weak $\lambda 8694.6$ S I line have been overestimated due to fringing residuals in their spectra. In general, more precise S abundances can be derived from the $\lambda \lambda 9212.9, 9237.5$ lines as they are more easily detected and less susceptible to observational uncertainties. In this connection, it should be noted that Caffau et al. find a few stars to have very high $[\text{S}/\text{Fe}]$ values even on the basis of these lines. Most remarkable is BD +02°263, for which they get $[\text{S}/\text{Fe}] = +0.91$. This star is, however, a single-lined spectroscopic binary according to Latham et al. (2002), which may have affected the determination of T_{eff} and $\log g$ and hence the abundances of S and Fe.

4.2.4. 3D and non-LTE effects on the S I lines

In Paper I it was shown that the application of 3D hydrodynamical model atmospheres instead of classical 1D models has a rather small effect on the derived sulphur abundance (see also Asplund 2005). For the large majority of our stars, 3D models lead to an increase of $\log \epsilon(\text{S})$ by 0.05 to 0.10 dex. This increase is, however, compensated by about the same increase in iron abundance (see Table 5 in Paper I for details). Hence, $[\text{S}/\text{Fe}]$ is practically unchanged.

It was noted in Paper I that the good agreement between S abundances derived from the weak $\lambda 8694.6$ S I line and the stronger $\lambda \lambda 9212.9, 9237.5$ lines suggests that non-LTE effects on the sulphur lines are small. Thanks to the recent non-LTE calculations of Takeda et al. (2005), this statement may now be quantified. From extensive statistical equilibrium calculations Takeda et al. show that the $\lambda \lambda 9212.9, 9237.5$ lines can suffer from significant negative non-LTE corrections, whereas the non-LTE effects on the $\lambda 8694.6$ line are small. The size of the corrections depend on the rate of inelastic collisions with neutral hydrogen, for which Takeda et al. adopt the classical approximation of Drawin (1968, 1969) in the version of Steenbock & Holweger

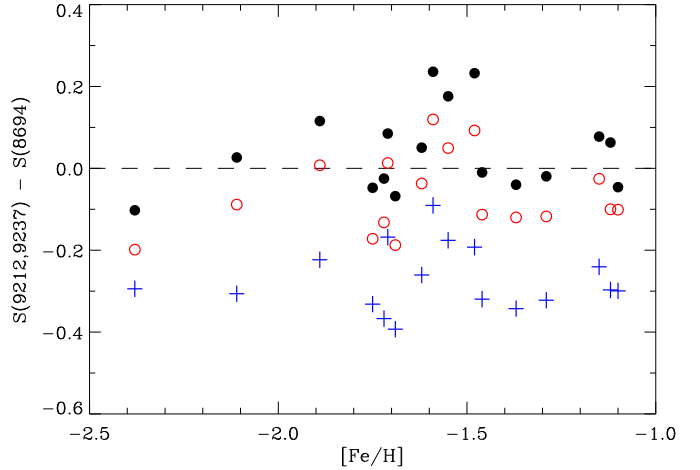


Fig. 8. Comparison of S abundances derived from the S I 9212.9, 9237.5 Å pair and the $\lambda 8694.6$ line. Filled circles refer to LTE. Open circles include non-LTE corrections according to Takeda et al. (2005) with the hydrogen collisional parameter $S_{\text{H}} = 1$, and crosses refer to $S_{\text{H}} = 0.1$.

(1984) with a scaling factor S_{H} that is varied from 10^{-3} to 10.

As seen from the tables of Takeda et al. (2005), the non-LTE effects vary quite strongly with T_{eff} , $\log g$ and $[\text{Fe}/\text{H}]$, but interpolation in the tables allows us to derive non-LTE corrections for our set of stars. In Fig. 8, the resulting difference of the S abundance derived from the $\lambda 9212.9, 9237.5$ Å pair and the $\lambda 8694.6$ line has been plotted for two values of S_{H} and also in the LTE case. As seen, both LTE and $S_{\text{H}} = 1$ give a satisfactory agreement between the two sets of S abundances, whereas the case of $S_{\text{H}} = 0.1$ can be excluded. The average difference and dispersion of $\log \epsilon(\text{S})_{9212,9237} - \log \epsilon(\text{S})_{8694}$ are as follows: $+0.04 \pm 0.10$ (LTE), -0.06 ± 0.09 (non-LTE with $S_{\text{H}} = 1$), and -0.27 ± 0.08 (non-LTE with $S_{\text{H}} = 0.1$). This suggests that hydrogen collisions are quite efficient in thermalizing the S I atoms. Still, the non-LTE effects for the $\lambda \lambda 9212.9, 9237.5$ lines may be of importance for the derived $[\text{S}/\text{Fe}]$ trend, due to varying non-LTE abundance corrections as a function of $[\text{Fe}/\text{H}]$. In the case of $S_{\text{H}} = 1$, the corrections obtained by Takeda et al. range from about -0.06 dex for the coolest of our stars to about -0.25 dex for the hottest and most metal-poor stars (e.g. G 64-12).

4.2.5. CRIRES observations of the $1.046 \mu\text{m}$ S I triplet

As part of the science verification of the ESO/VLT Cryogenic high-resolution IR Echelle Spectrograph, CRIRES (Käuffl et al. 2004), a spectrum around the $1.046 \mu\text{m}$ S I triplet was obtained for G 29-23 ($V = 10.19$, $[\text{Fe}/\text{H}] = -1.69$) on October 6, 2006. The entrance slit width of CRIRES was set at 0.4 arcsec, which corresponds to a resolution of $\lambda/\Delta\lambda \simeq 50\,000$ with four detector pixels per spectral resolution bin $\Delta\lambda$. In order to improve removal of sky emission and detector dark current, the observations were performed in nodding mode with a shift of 10 arcsec between the two settings of the star in the slit. The exposure time was 2400 sec. The seeing was rather poor (about 1.3 arcsec) but adaptive optics was applied to improve the stellar image, and the combined

Table 2. Atomic data for the $1.046\ \mu\text{m}$ S I triplet. Column 5 lists the equivalent width in the spectrum of G 29-23 and the last column gives the derived LTE sulphur abundance.

	Wavelength \AA	Exc.Pot. eV	$\log gf$	$W_\lambda(\text{G29-23})$ m \AA	$\log \epsilon(\text{S})$
S I	10455.5	6.86	0.26	39.5	5.82
S I	10456.8	6.86	-0.44	10.1	5.75
S I	10459.4	6.86	0.03	25.7	5.77

spectrum has a very satisfactory S/N of 330 per spectral dispersion pixel. For comparison, we note that our UVES spectrum of G 29-23 (exposure time 1800 sec) has S/N ~ 200 around the S I lines at $9212\text{--}9238\ \text{\AA}$.² Furthermore, unlike the UVES near-IR spectrum, the CRIRES spectrum at $1.046\ \mu\text{m}$ is not plagued by telluric lines and fringing residuals.

The CRIRES data was reduced by using standard IRAF tasks for subtraction of bias and dark, spectrum extraction, and wavelength calibration. Note that CRIRES supports high accuracy wavelength calibration by means of a Th-Ar hollow cathode lamp (Kerber et al. 2006). Flatfielding was performed by the aid of the extracted spectrum of the bright ($V = 4.28$) B9III star HD 15315. The resulting spectrum of G 29-23 is shown in Fig. 9 and compared with a spectral synthesis of the three sulphur lines.

Atomic data for the $1.046\ \mu\text{m}$ S I triplet are given in Table 2 together with the measured equivalent widths in the G 29-23 spectrum. As in the case of the other S I lines the gf values were taken from Lambert & Luck (1978) and collisional broadening data are from Barklem et al. (2000b). The derived LTE S abundances given in Table 2 agree very well with the S abundances derived from the S I lines observed with UVES. An average of $[\text{S}/\text{Fe}] = +0.29$ is obtained from the UVES lines and $[\text{S}/\text{Fe}] = +0.27$ from the CRIRES lines. For all six S I lines the mean sulphur abundances is $\log \epsilon(\text{S}) = 5.79$ and the rms deviation is only 0.035 dex. Although one should not put too much weight on a single star, we consider this good agreement to be an important check of the reliability of our sulphur abundance determinations.

According to Takeda et al. (2005), the non-LTE corrections for the $1.046\ \mu\text{m}$ S I triplet are somewhat smaller than in the case of the $\lambda\lambda 9212.9, 9237.5\ \text{\AA}$ lines. Hence, one might in principle also use the $1.046\ \mu\text{m}$ triplet to study non-LTE effects and calibrate the S_{H} parameter like we did when comparing S abundances from the $\lambda 8694.6$ line and the $\lambda\lambda 9212.9, 9237.5$ pair. This would, however, require IR observations for many more stars to provide statistically significant results.

4.3. Zinc

The Zn abundances are derived from the equivalent widths of the two Zn I lines at 4722.2 and $4810.5\ \text{\AA}$. Adopted gf values (see Table A.1) are from Biémont & Godefroid (1980), and collisional broadening data were taken from Barklem et al. (2000b). In Paper I, a solar Zn abundance of $\log \epsilon(\text{Zn})_{\odot} =$

² The UVES spectra also cover the $1.046\ \mu\text{m}$ S I triplet but due to the low efficiency of the MIT CCD at this wavelength, the quality is far too low ($S/N < 25$) for a precise determination of the sulphur abundance.

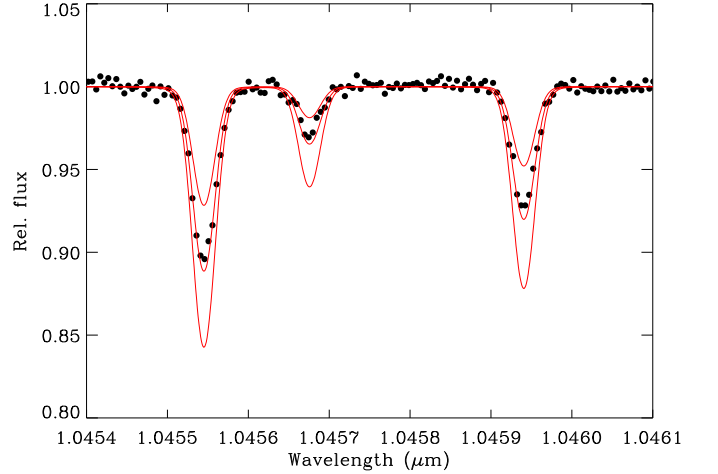


Fig. 9. The CRIRES spectrum of G 29-23 around the $1.046\ \mu\text{m}$ S I triplet (dots) compared with synthetic profiles for three sulphur abundances, $\log \epsilon(\text{S}) = 5.51, 5.81$ and 6.11 corresponding to $[\text{S}/\text{Fe}] = 0.0, 0.3$ and 0.6 , respectively. As seen, the $[\text{S}/\text{Fe}] = 0.3$ case provides an excellent fit to the observations.

4.57 was derived from the two lines, but this value is sensitive to the solar microturbulence parameter. Here, we adopt $\log \epsilon(\text{Zn})_{\odot} = 4.60$ as derived by Biémont & Godefroid (1980) from six Zn I lines. This value is in good agreement with the meteoritic value, $\log \epsilon(\text{Zn}) = 4.61 \pm 0.04$ (Asplund et al. 2005).

As seen from Table A.1, the zinc lines are very weak in turnoff stars with metallicities below -2 . The equivalent widths are on the order of $2\text{--}3\ \text{m\AA}$ in stars with $[\text{Fe}/\text{H}] \sim -2.5$. Still, the Zn lines can be clearly detected at metallicities below -3 as seen from Fig. 10. This is connected to the fact that the Zn/Fe ratio appears to rise steeply below $[\text{Fe}/\text{H}] \sim -3$.

Takeda et al. (2005) have also performed non-LTE calculations for the $\lambda\lambda 4722.2, 4810.5$ Zn I lines. Generally, the absolute value of the non-LTE corrections are smaller than in the case of the $\lambda\lambda 9212.9, 9237.5$ S I lines, and they have opposite sign. For a typical metal-poor turnoff star, the non-LTE correction of the zinc abundance is on the order of $+0.10$ dex, whereas the correction is -0.25 dex for the sulphur abundance. For cooler and more metal-rich stars the non-LTE corrections on zinc are less than 0.1 dex. These corrections refer to a hydrogen collisional parameter $S_{\text{H}} = 1$, and increase somewhat if $S_{\text{H}} < 1$.

As discussed in Paper I, the absolute values of the 3D corrections of the Zn abundances are less than 0.1 dex and they are similar to the 3D corrections of the Fe abundances based on Fe II lines. Hence, the derived Zn/Fe ratio would not change significantly (at least not under the assumption of LTE) if 3D models were applied.

5. Results and discussion

5.1. S/Fe vs. Fe/H

The derived sulphur abundances are given in Table 1. In the calculation of $[\text{S}/\text{Fe}]$, solar abundances $\log \epsilon(\text{S})_{\odot} = 7.20$ and $\log \epsilon(\text{Fe})_{\odot} = 7.50$ were adopted. Had we instead applied the newest solar abundances, $\log \epsilon(\text{S})_{\odot} = 7.14$ and $\log \epsilon(\text{Fe})_{\odot} = 7.45$, determined by Asplund et al. (2005), the $[\text{S}/\text{Fe}]$ values would have increased by only 0.01 dex.

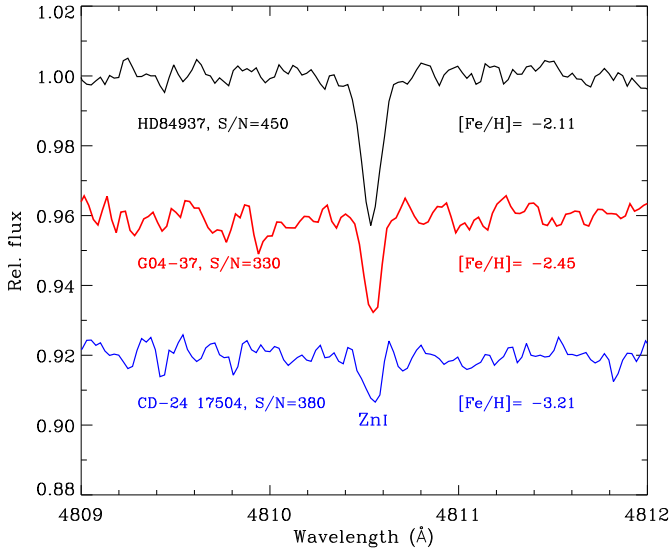


Fig. 10. The $\lambda 4810.5$ Zn I line in UVES spectra of three stars. The spectra of G 04-37 and CD $-24^\circ 17504$ have been offset in relative flux by 0.04 and 0.08, respectively.

The $[\text{S}/\text{Fe}]$ values in Table 1 are plotted vs. $[\text{Fe}/\text{H}]$ in Fig. 11 together with data for 25 disk stars from Chen et al. (2002). The error bars shown refer to the $1\text{-}\sigma$ statistical error caused by the uncertainty of the observed equivalent widths and the atmospheric parameters of the stars. In the case of $[\text{Fe}/\text{H}]$, which is based on many Fe II lines, the dominating error comes from the uncertainty of the gravity; $\sigma(\log g) = 0.15$ dex corresponds to $\sigma[\text{Fe}/\text{H}] = 0.05$ dex (see Table 4 in Paper I). The $\log g$ induced error of $[\text{S}/\text{Fe}]$ is, on the other hand, negligible, because a change in gravity has nearly the same effect on S and Fe abundances. In the case of $[\text{S}/\text{Fe}]$ the major error contribution comes from the uncertainty of T_{eff} and the error of the equivalent width measurements. For the three most metal-poor stars with $[\text{Fe}/\text{H}] < -3$, the W_λ induced error becomes particularly large, because only the $\lambda 9212.9$ S I line is strong enough to be detected and it is as weak as $W_\lambda \sim 5$ mÅ.

As seen from Fig. 11, the LTE values of $[\text{S}/\text{Fe}]$ suggest a small slope of $[\text{S}/\text{Fe}]$ as a function of $[\text{Fe}/\text{H}]$, whereas the non-LTE values give a nearly flat relation. The mean $[\text{S}/\text{Fe}]$ and the rms deviation for the halo stars are:

$$\begin{aligned} \langle [\text{S}/\text{Fe}] \rangle &= 0.319 \pm 0.078 \text{ in the LTE case, and} \\ \langle [\text{S}/\text{Fe}] \rangle &= 0.208 \pm 0.067 \text{ in the non-LTE case.} \end{aligned}$$

We note that the four single-lined spectroscopic binaries (see Table 1) do not show any particular large or systematic deviations from the mean value of $[\text{S}/\text{Fe}]$.

The trend of $[\text{S}/\text{Fe}]$ in Fig. 11 corresponds rather well to analogous trends recently derived for $[\text{Mg}/\text{Fe}]$, $[\text{Si}/\text{Fe}]$ and $[\text{Ca}/\text{Fe}]$ (Jonsell et al. 2005, Gehren et al. 2006). Qualitatively, our data also agree with the trend of $[\text{S}/\text{Fe}]$ predicted from models of the chemical evolution of our Galaxy. Based on the Woosley & Weaver (1995) yields of Type II SNe, Goswami & Prantzos (2000) obtain a near-constant level $[\text{S}/\text{Fe}] \sim +0.4$ in the metallicity range $-3 < [\text{Fe}/\text{H}] < -1$ and a decline of $[\text{S}/\text{Fe}]$ for $[\text{Fe}/\text{H}] > -1$ due to the additional supply of iron from Type Ia SNe. Chiappini et al. (1999), on the other hand, obtain a slope of $[\text{S}/\text{Fe}]$ in the range $-3 < [\text{Fe}/\text{H}] < -1$ like the one we determine in the LTE case, because they assume that Type

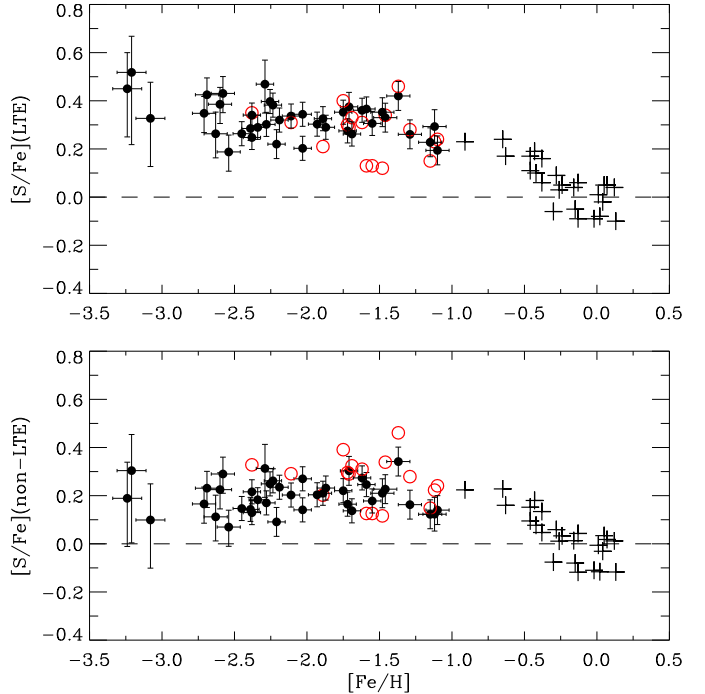


Fig. 11. $[\text{S}/\text{Fe}]$ vs. $[\text{Fe}/\text{H}]$ for our sample of halo stars supplemented with disk stars (shown as crosses) from Chen et al. (2002). Filled circles with error bars show data based on S abundances derived from the $\lambda\lambda 9212.9, 9237.5$ S I lines, and open circles show data based on the weak $\lambda 8694.6$ S I line. In the upper panel LTE has been assumed in deriving the S abundances, whereas the lower panel includes non-LTE corrections from Takeda et al. (2005) with the hydrogen collisional parameter $S_{\text{H}} = 1$. In both cases, the iron abundances are the LTE values derived from Fe II lines.

Ia SNe start contributing with iron already in the Galactic halo phase. Finally, Kobayashi et al. (2006) predict a level of $[\text{S}/\text{Fe}] \sim +0.4$ based on new yield calculations in a model where hypernovae are assumed to have the same frequency as Type II SNe. We note that our data do not allow us to establish conclusively whether a small slope of $[\text{S}/\text{Fe}]$ is present or not due to the uncertainty about the non-LTE corrections. It should also be noted that the predicted level of $[\text{S}/\text{Fe}]$ among halo stars depends critically on the assumed mass cut between the ejecta and the collapsing core in massive SNe. Hence, any detailed comparison between observed and predicted trends of $[\text{S}/\text{Fe}]$ seems somewhat premature.

It is interesting to compare the observed scatter of $[\text{S}/\text{Fe}]$ with the scatter predicted from stochastic chemical evolution models. In sharp contrast to the results of Caffau et al. (2005), we find a very small scatter (± 0.07 dex) of $[\text{S}/\text{Fe}]$ among the halo stars, and there is no indication that the scatter increases significantly towards the most metal-poor stars. This scatter is not much higher than expected from the observational errors of $[\text{S}/\text{Fe}]$. Hence, the cosmic scatter in $[\text{S}/\text{Fe}]$ at a given $[\text{Fe}/\text{H}]$ must be less than 0.07 dex. A similar low scatter has been obtained for other α -capture elements, when high precision and homogeneous data have become available. Nissen et al. (1994) found the scatter of Mg, Ca and Ti relative to Fe to be < 0.06 dex in the metallicity range $-3 < [\text{Fe}/\text{H}] < -1.5$. More recently, Arnone et al. (2005) found the cosmic scatter of

$[\text{Mg}/\text{Fe}]$ to be < 0.06 dex for 25 turnoff stars in the range $-3.2 < [\text{Fe}/\text{H}] < -2^3$. At still lower metallicities, Cayrel et al. (2004) find a scatter of 0.10 - 0.15 dex for $[\text{Mg}/\text{Fe}]$, $[\text{Si}/\text{Fe}]$, $[\text{Ca}/\text{Fe}]$ and $[\text{Ti}/\text{Fe}]$ for 30 giant stars ranging in $[\text{Fe}/\text{H}]$ from -4.1 to -2.7 . A similar low scatter of these ratios has been derived by Cohen et al. (2004) for 28 dwarf stars in the metallicity range $-3.6 < [\text{Fe}/\text{H}] < -2.0$.

The observed scatter of α -capture elements relative to Fe is much smaller than predicted from stochastic models of the chemical evolution of metal-poor systems (Argast et al. 2000, 2002, Karlsson & Gustafsson 2005). This is connected to the fact that calculated yields of Type II SNe vary strongly with progenitor mass. According to Nomoto et al. (1997), the yield ratio S/Fe increases by a factor of 12 when the progenitor mass is changed from 13 to 40 solar masses. Hence, in the early Galaxy, where only a few supernovae enrich the interstellar gas of a star-forming cloud according to current models, one would expect a much higher scatter in $[\text{S}/\text{Fe}]$ than the derived value of < 0.07 dex for our sample of stars. Sulphur has not been specifically modelled in any of the stochastic models, but in the case of Si that has similar yield variations as S, Argast et al. (2000) predict a rms scatter of ± 0.35 dex at $[\text{Fe}/\text{H}] = -3.0$, ± 0.25 dex at $[\text{Fe}/\text{H}] = -2.5$, and ± 0.12 dex at $[\text{Fe}/\text{H}] = -2.0$. As discussed in detail by Arnone et al. (2005) and Karlsson & Gustafsson (2005), possible explanations of this discrepancy are: *i*) The calculated yield ratios are wrong, i.e. the released amount of alpha-elements relative to Fe is nearly independent of progenitor mass, *ii*) the IMF is biased to a narrow mass range in the early Galaxy, and *iii*) the mixing of SNe ejecta is much more rapid than assumed in the models, such that a large number of SNe always contribute to the enrichment of a cloud. The last possibility means that the mixing time scale of supernova ejecta is considerably shorter than the cooling time of star-forming gas clouds.

It should be noted that the scatter in the abundance of α -capture elements relative to Fe probably increases towards the more metal-rich end of the halo. Paper I includes six halo stars with $[\text{Fe}/\text{H}] > -1$, four of which have $[\text{S}/\text{Fe}] \simeq +0.3$ and two have $[\text{S}/\text{Fe}] \simeq 0.0$. This scatter is in accordance with the results of Nissen & Schuster (1997), who find a similar dichotomy in $[\alpha/\text{Fe}]$ for halo stars with $-1 < [\text{Fe}/\text{H}] < -0.6$. As suggested in their paper, the explanation of the scatter may be that the metal-rich α -poor stars have formed in the outer regions of the Galaxy where the star formation has proceeded so slowly that iron from Type Ia SNe has been incorporated in them. Supporting evidence has been obtained by Gratton et al. (2003), who find $[\alpha/\text{Fe}]$ to be lower and more scattered in stars belonging to the ‘accretion’ component of the Galaxy than in stars belonging to the ‘dissipative’ component.

5.2. Zn/Fe vs. Fe/H

The LTE values of $[\text{Zn}/\text{Fe}]$ are plotted as a function of $[\text{Fe}/\text{H}]$ in the upper panel of Fig. 12. In the lower panel, non-LTE corrections of $[\text{Zn}/\text{Fe}]$ from Takeda et al. (2005) have been included. The error bars refer to the $1\text{-}\sigma$ statistical

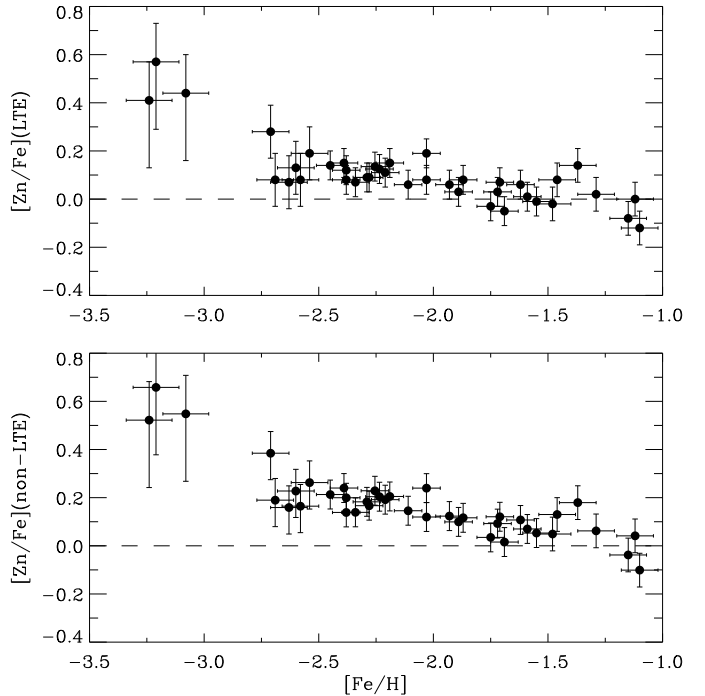


Fig. 12. $[\text{Zn}/\text{Fe}]$ vs. $[\text{Fe}/\text{H}]$ for our sample of halo stars. The upper panel refers to LTE Zn abundances. The lower panel includes non-LTE corrections from Takeda et al. (2005) corresponding to a hydrogen collisional parameter $S_{\text{H}} = 1$.

error caused by the uncertainty of the observed equivalent widths and the atmospheric parameters of the stars. For the three most metal-poor stars, the W_{λ} -induced error is large, because the equivalent widths of the Zn I lines are only about $1 \text{ m}\text{\AA}$.

As seen from the upper panel of Fig. 12, the LTE values of $[\text{Zn}/\text{Fe}]$ are close to zero in the metallicity range $-2 < [\text{Fe}/\text{H}] < -1$. In the range $-2.7 < [\text{Fe}/\text{H}] < -2$, all $[\text{Zn}/\text{Fe}]$ values are, however, positive with an average value of $[\text{Zn}/\text{Fe}] \simeq +0.1$. Furthermore, $[\text{Zn}/\text{Fe}]$ seems to rise steeply below $[\text{Fe}/\text{H}] = -3$ to a value of $[\text{Zn}/\text{Fe}] \sim +0.5$. This trend is reinforced if non-LTE corrections corresponding to $S_{\text{H}} = 1$ are applied, because the corrections to $[\text{Zn}/\text{Fe}]$ are positive and increase with decreasing $[\text{Fe}/\text{H}]$. Unlike the case of sulphur, we had no possibility to calibrate the S_{H} parameter for zinc (our two Zn I lines have nearly the same excitation potential), but we note that if $S_{\text{H}} < 1$ (corresponding to a lower efficiency of thermalizing the Zn atoms by inelastic collisions with hydrogen atoms) then the non-LTE corrections for the metal-poor stars would be still larger.

The trend of $[\text{Zn}/\text{Fe}]$ in Fig. 12 (LTE case) corresponds very well to the trend found by Cayrel et al. (2004) from an LTE analysis of the $\lambda\lambda 4722.2, 4810.5$ Zn I lines in UVES spectra of 35 giant stars with $-4.2 < [\text{Fe}/\text{H}] < -2$. Hence, there can be little doubt that Zn is indeed overabundant with respect to iron for very metal-poor stars, especially because the possible non-LTE corrections go in the direction of making the overabundance larger.

Zinc is a key element in recent studies of nucleosynthesis and chemical evolution in the early Galaxy (Umeda & Nomoto 2003, 2005; Nomoto et al. 2006; Kobayashi et al. 2006). As shown by Kobayashi et al. (2006), traditional

³ This range is on our metallicity scale. The metallicities of Arnone et al. (2005) are based on Fe I lines and a T_{eff} scale that is on the average $\sim 200 \text{ K}$ lower than our scale. For 14 stars in common with our sample, they get $[\text{Fe}/\text{H}]$ values that are on the average 0.20 dex lower than our values.

yields of Type II SNe (Nomoto et al. 1997) correspond to $[\text{Zn}/\text{Fe}] \sim -1$, i.e. far below the observed values of $[\text{Zn}/\text{Fe}]$. In order to explain a level of $[\text{Zn}/\text{Fe}]$ around zero, one has to invoke models of hypernovae, i.e. core collapse SNe with explosion energy $E \gtrsim 10^{52}$ ergs. Furthermore, a mixing and fallback mechanism or an asymmetric explosion (Maeda & Nomoto 2003) has to be introduced in order to bring up sufficient Zn from layers with complete Si burning. By including such hypernovae with a frequency of 50% relative to Type II SNe and a Salpeter IMF, Kobayashi et al. (2006) predict $[\text{Zn}/\text{Fe}] \sim 0.1$ in the Galactic halo. The upturn of $[\text{Zn}/\text{Fe}]$ at the lowest metallicities is, however, not predicted. In order to explain $[\text{Zn}/\text{Fe}] \gtrsim +0.3$, Nomoto et al. (2006) suggest that stars with $[\text{Fe}/\text{H}] < -3$ have been formed from the ejecta of Pop. III hypernovae with very large explosion energy. Another possibility for high Zn/Fe production is from core-collapsing, very massive stars with $M \sim 500 - 1000 M_{\odot}$ (Ohkubo et al. 2006).

5.3. S/Zn vs. Zn/H

As explained in the Introduction, the S/Zn ratio is potentially of great value in the analysis of the metallicities of distant galaxies detected via the absorption lines they produce in the spectra of quasars; the damped Lyman-alpha systems (DLAs) are a particularly important subset of such absorbers (Wolfe et al. 2005). The role of S and Zn in these studies stems from the fact that both elements have a low condensation temperature and are not expected to be significantly depleted onto dust. This is not the case, for example, for refractory elements such as Si and Fe. Indeed, one of the motivations for the present study was to use the behaviour of $[\text{S}/\text{Zn}]$ vs. $[\text{Zn}/\text{H}]$ in Galactic stars as a guide to the interpretation of the star formation history of high redshift galaxies.

Figure 13 shows $[\text{S}/\text{Zn}]$ vs. $[\text{Zn}/\text{H}]$ for our halo stars except the three with $[\text{Fe}/\text{H}] < -3$, which have such large errors in both S and Zn that the ratio S/Zn becomes very uncertain. In addition, we have included six halo stars with $-1.1 < [\text{Zn}/\text{H}] < -0.6$ from Paper I and 14 disk stars with S and Zn abundances from Chen et al. (2002; 2004). The upper panel shows LTE values; in the lower panel non-LTE corrections ($S_{\text{H}} = 1$) from Takeda et al. (2005) have been applied. By comparing the two panels, the importance of the non-LTE corrections is readily apparent. When the corrections are applied, there is an overall decrease in $[\text{S}/\text{Zn}]$ at all but the highest values of $[\text{Zn}/\text{H}]$ considered here. Furthermore, non-LTE effects are most significant at low metallicities with the result that, apparently, $[\text{S}/\text{Zn}]$ reverts to solar values when $[\text{Zn}/\text{H}] \lesssim -2$. Such behaviour is unusual but, given our current limited understanding of the nucleosynthesis of Zn, cannot be excluded.

Taken at face value, the lack of a strong metallicity trend in the lower panel of Fig. 13 would indicate that the usefulness of the S/Zn ratio as a ‘clock’ of the star-formation history is rather limited—departures from the solar value are generally small and, in particular, not much greater than the typical measurement error in DLAs. In Table C.1 we have collected all published, or about to be published, measurements of $[\text{S}/\text{Zn}]$ in DLAs secured with echelle spectrographs on 8-10m class telescopes. In comparison with the corresponding table in Paper I, the number of DLAs with accurate measures of the abundances of sulphur and

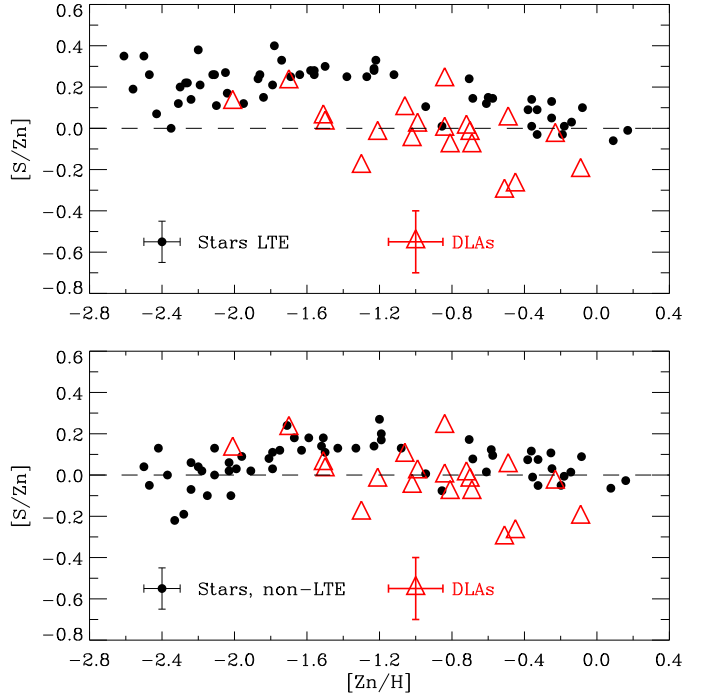


Fig. 13. $[\text{S}/\text{Zn}]$ vs. $[\text{Zn}/\text{H}]$ for Galactic stars and damped Lyman-alpha systems. Typical $1\text{-}\sigma$ error bars are shown.

zinc has doubled since 2004, from 10 to 20. These data are shown as triangles in Fig. 13.

Whereas in previous papers (e.g. Paper I) a systematic difference had been noted between the $[\text{S}/\text{Zn}]$ ratio in Galactic metal-poor stars and in DLAs of comparable metallicities (evident in the top panel of Fig. 13), the situation is considerably less clear-cut if one adopts the non-LTE corrections to the abundances of S and Zn. If these corrections are appropriate, it would explain why so few DLAs show enhanced $[\text{S}/\text{Zn}]$ values, when other ratios of alpha-capture to iron-peak elements apparently do, once dust depletions are accounted for (e.g. Prochaska & Wolfe 2002). A minor difference – which needs to be quantified with larger datasets – between Galactic stars and DLAs is the larger scatter in the $[\text{S}/\text{Zn}]$ ratio possibly exhibited by the latter. It is intriguing, in particular, to find an *underabundance* of S relative to Zn in some DLAs with relatively high overall metallicities. If confirmed, the larger dispersion of the ratio in DLAs could be an indication that, as one might expect, the host galaxies of DLAs experienced a variety of different star formation histories, and don’t necessarily follow closely the abundance trends seen in a *single* galaxy like the Milky Way.

6. Summary and conclusions

High S/N UVES spectra of 40 metal-poor halo stars have been used to derive S, Fe and Zn abundances. For one star we also present novel observations of the Si I triplet at $1.046 \mu\text{m}$ carried out with the ESO VLT CRIRES spectrograph. These data confirm the S abundance obtained from other Si I lines and demonstrates the high efficiency of CRIRES in obtaining high-resolution infrared spectra.

From the results presented in this paper, we conclude that $[\text{S}/\text{Fe}]$ in Galactic halo stars shows the same kind of

dependence on $[\text{Fe}/\text{H}]$ as $[\text{Mg}/\text{Fe}]$, $[\text{Si}/\text{Fe}]$ and $[\text{Ca}/\text{Fe}]$, i.e. a near-constant ratio at a level of $+0.2$ to $+0.3$ dex. This strongly suggests that sulphur in the Galactic halo was made by α -capture processes in massive SNe, as predicted from current models of Galactic chemical evolution with yields calculated for hydrostatic and explosive oxygen and silicon burning.

Among the 40 halo stars observed, we do not find a single case of the high S/Fe ratios ($[\text{S}/\text{Fe}] > 0.60$) claimed in some recent papers (Israelian & Rebolo 2001; Takada-Hidai et al. 2002; Caffau et al. 2005). The majority of these high values were based on the very weak $\lambda 8694.6$ S I line and, as shown in Sect. 4.2, our very high S/N, fringe-corrected spectra do not confirm the claimed strength of this line in three metal-poor main-sequence stars. A more convincing detection of the $\lambda 8694.6$ S I line has been obtained by Israelian & Rebolo (2001) for two giant stars, HD 2665 and HD 2796 with $[\text{Fe}/\text{H}] = -2.0$ and -2.3 . The derived $[\text{S}/\text{Fe}]$ values are $+0.69$ and $+0.81$ dex, respectively. Further studies of S abundances in such metal-poor giant stars would be interesting, especially if one could use the forbidden sulphur line at $1.082 \mu\text{m}$, which is expected to be insensitive to non-LTE effects.

From an observational point of view, the $\lambda\lambda 9212.9, 9237.5$ pair of S I lines or the S I triplet at $1.046 \mu\text{m}$ provide more precise values of the S abundance than the weak $\lambda 8694.6$ S I line, but according to Takeda et al. (2005) these stronger lines are quite sensitive to departures from LTE. The size of the non-LTE effects depends on the efficiency of inelastic collisions with neutral hydrogen. Adopting the classical formula of Drawin (1968, 1969) with a scaling parameter S_{H} , a comparison of S abundances from the $\lambda 8694.6$ line and the $\lambda\lambda 9212.9, 9237.5$ pair points to $S_{\text{H}} \gtrsim 1$, which means that we are not too far away from LTE. Nevertheless, the non-LTE corrections may be of importance for the derived trend of $[\text{S}/\text{Fe}]$ as seen from Fig. 11. Hence, it would be important to perform improved quantum mechanical calculations for inelastic S + H collisions as has been achieved for Li + H collisions (Belyaev & Barklem 2003).

An interesting and robust result of our investigation is the small scatter of $[\text{S}/\text{Fe}]$ at a given metallicity. It is found to be around ± 0.07 dex in the whole range $-3.2 < [\text{Fe}/\text{H}] < -1$. A similarly low scatter has been found for the other α -capture elements, i.e. $[\text{Mg}/\text{Fe}]$, $[\text{Si}/\text{Fe}]$, and $[\text{Ca}/\text{Fe}]$ (Cayrel et al. 2004; Cohen et al. 2004). Current stochastic models of the chemical evolution of metal-poor systems (Argast et al. 2000, 2002, Karlsson & Gustafsson 2005) predict a much higher scatter of $[\alpha/\text{Fe}]$ for metallicities below -2 . Clearly the models and/or calculated yield ratios of massive SNe need to be revised.

Zinc is found to be slightly overabundant with respect to Fe in the metallicity range $-3 < [\text{Fe}/\text{H}] < -2$. Below $[\text{Fe}/\text{H}] \sim -3$, $[\text{Zn}/\text{Fe}]$ increases rapidly to a level of $+0.5$ dex. Hence, our study of main-sequence halo stars confirms the upturn of Zn/Fe previously found for very metal poor giants (Primas et al. 2000; Johnson & Bolte 2001; Cayrel et al. 2004). The high value of Zn/Fe at the lowest metallicities may be a signature that stars with $[\text{Fe}/\text{H}] < -3$ have been made from the ejecta of hypernovae with very large explosion energy as suggested by Nomoto et al. (2006). However, our understanding of the nucleosynthesis of Zn at all metallicities is still very limited.

Finally, we find a much reduced ‘signal’ in the $[\text{S}/\text{Zn}]$ ratio as a tracer of the previous history of star formation, if non-LTE effects to the abundances of these two elements are taken into account. It would be very desirable to perform a check of the validity of the non-LTE corrections to the Zn abundance by comparing lines arising from levels with different excitation potentials, as we have been able to do here for S. However, if the non-LTE corrections applied are appropriate, it would explain why in general DLAs do not exhibit markedly supersolar $[\text{S}/\text{Zn}]$ ratios, even at metallicities comparable to those of Galactic halo stars.

Acknowledgements. The ESO staff at Paranal is thanked for carrying out the VLT/UVES service observations. We acknowledge help from Francesca Primas, Hughes Sana, Lowell Tacconi-Garman and Burkhard Wolff in obtaining the CRIRES spectrum of G 29-23. Paul Barklem is thanked for providing a version of the BSYN program including the hydrogen lines. We are grateful to Miroslava Dessauges-Zavadsky, Sara Ellison and Jason Prochaska for communicating measurements of $[\text{S}/\text{Zn}]$ in DLAs in advance of publication. This publication made use of the SIMBAD database operated at CDS, Strasbourg, France, and of data products from the Two Micron All Sky Survey, which is a joint project of the University of Massachusetts and the Infrared Processing and Analysis Center/California Institute of Technology, funded by NASA and the National Science Foundation. This research has made use of NASA’s Astrophysics Data System.

References

- Alonso, A., Arribas, S., & Martínez-Roger, C. 1994, *A&AS*, 107, 365
 Alonso, A., Arribas, S., & Martínez-Roger, C. 1995, *A&A*, 297, 197
 Alonso, A., Arribas, S., & Martínez-Roger, C. 1996, *A&A*, 313, 873
 Argast, D., Samland, M., Gerhard, O.E., & Thielemann, F.-K. 2000, *A&A*, 356, 873
 Argast, D., Samland, M., Thielemann, F.-K., & Gerhard, O.E. 2002, *A&A*, 388, 842
 Arnone, E., Ryan, S.G., Argast, D., Norris, J.E., & Beers, T.C. 2005, *A&A*, 430, 507
 Asplund, M. 2005, *ARA&A*, 43, 481
 Asplund, M., Grevesse, N., & Sauval, A.J. 2005, in: *Cosmic abundances as records of stellar evolution and nucleosynthesis*, eds T.G. Barnes III and F.N. Bash, ASP Conf. series vol. 336, p. 25
 Asplund, M., Gustafsson, B., Kiselman, D., & Eriksson, K. 1997, *A&A*, 318, 521
 Asplund, M., Lambert, D.L., Nissen, P.E., Primas, F., & Smith, V.V. 2006, *ApJ*, 644, 229
 Barklem, P.S. 2007, *A&A*, 466, 327
 Barklem, P.S., & Asplund-Johansson, J. 2005, *A&A*, 435, 373
 Barklem, P.S., Piskunov, N., & O’Mara, B.J. 2000a, *A&A*, 363, 1091
 Barklem, P.S., Piskunov, N., & O’Mara, B.J. 2000b, *A&AS*, 142, 467
 Barklem, P.S., Stempels, H.C., Allende Prieto, C., et al. 2002, *A&A*, 385, 951
 Bagnulo, S., Jehin, E., Ledoux, C., et al. 2003, *ESO Messenger*, 114, 10
 Beers, T.C., Rossi, S., Norris, J.E., Ryan, S.G., & Sheffer, T. 1999, *AJ*, 117, 981
 Belyaev, A.K., & Barklem, P.S. 2003, *PhRvA*, 68, 062703
 Biémont, E., & Godefroid, M. 1980, *A&A*, 84, 361
 Biémont, E., Quinet, P., & Zeppen, C.J. 1993, *A&AS*, 102, 435
 Bridges, J.M., & Wiese, W.L. 1967, *Phys. Rev.*, 159, 31
 Caffau, E., Bonifacio, P., Faraggiana, R., et al. 2005, *A&A*, 441, 533
 Carney, B.W., Latham, D.W., Laird, J.B., Grant, C.E., & Morse, J.A. 2001, *AJ*, 122, 3419
 Cayrel, R., Depagne, E., Spite, M. et al. 2004, *A&A*, 416, 1117
 Centurión, M., Molaro, P., Vladilo, G., et al. 2003, *A&A*, 403, 55
 Chen, Y.Q., Nissen, P.E., Zhao, G., & Asplund, M. 2002, *A&A*, 390, 225
 Chen, Y.Q., Nissen, P.E., & Zhao, G. 2004, *A&A*, 425, 697
 Chiappini, C., Matteucci, F., Beers, T.C., & Nomoto, K. 1999, *ApJ*, 515, 226
 Cohen, J.G., Christlieb, N., McWilliam, A., et al. 2004, *ApJ*, 612, 1107
 Cutri, R.M., Skrutskie, M.F., Van Dyk, S., et al. 2003, *Explanatory Supplement to the 2MASS All Sky Data*

- Release, (IPAC/California Institute of Technology); <http://www.ipac.caltech.edu/2mass>
- Dekker, H., D'Odorico, S., Kaufer, A., Delabre, B., & Kotzlowski, H. 2000, Proc. SPIE, 4008, 534
- Dessauges-Zavadsky, M., Calura, F., Prochaska, J. X., D'Odorico, S., & Matteucci, F. 2004, A&A, 416, 79
- Dessauges-Zavadsky, M., Prochaska, J. X., D'Odorico, S., Calura, F., & Matteucci, F. 2006, A&A, 445, 93
- Dessauges-Zavadsky, M., Prochaska, J. X., D'Odorico, S., Calura, F., & Matteucci, F. 2007, A&A, submitted
- Drawin, H.W. 1968, Z. Physik, 211, 404
- Drawin, H.W. 1969, Z. Physik, 225, 483
- Ellison, S. L., Hennawi, J.F., Martin, C.L., & Sommer-Larsen, J. 2007, MNRAS, in press (arXiv:0704.1816)
- Ellison, S.L., & Lopez, S. 2001, A&A, 380, 117
- ESA 1997, The Hipparcos and Tycho Catalogues, ESA SP-1200
- Elias, J.H., Frogel, J.A., Matthews, K., & Neugebauer, G. 1982, AJ, 87, 1029
- Fuhrmann, K., Axer, M., & Gehren, T. 1993, A&A, 271, 451
- Gehren, T., Shi, J.R., Zhang, H.W., Zhao, G., & Korn, A.J. 2006, A&A, 451, 1065
- Gratton, R.G., Caretta, E., Desidera, S. et al. 2003, A&A, 406, 131
- Goswami, A., & Prantzos, N. 2000, A&A, 359, 191
- Henyey, L., Vardya, M.S. & Bodenheimer, P. 1965, ApJ, 142, 841
- Israeli, G., & Rebolo, R. 2001, ApJ, 557, L43
- Jonsell, K., Edvardsson, B., Gustafsson, B. et al. 2005, A&A, 440, 321
- Johnson, H.L. 1966, ARA&A, 4, 193
- Johnson, J.A., & Bolte, M. 2001, Nucl. Phys. A, 688, 41c
- Karlsson, T., & Gustafsson, B. 2005, A&A, 436, 879
- Käuff, H.U., Ballester, P., Biereichel, P., et al. 2004, Proc. SPIE, 5492, 1218
- Kerber, F., Nave, G., Sansonetti, C.J., et al. 2006, in: Ground-based and Airborne Instrumentation for Astronomy, eds I. S. McLean and M. Iye. Proceedings of the SPIE, 6269, pp. 20
- Kobayashi, C., Umeda, H., Nomoto, K., Tominaga, N., & Ohkubo, T. 2006, ApJ, 653, 1145
- Korn, A.J., & Ryde, N. 2005, A&A, 443, 1029
- Lambert, D.L., & Luck, R.E. 1978, MNRAS, 183, 79
- Latham, D.W., Stefanik, R.P., Torres, G., et al. 2002, AJ, 124, 1144
- Ledoux, C., Srianand, R., & Petitjean, P. 2002, A&A, 392, 781
- Lopez, S., & Ellison, S. L. 2003, A&A, 403, 573
- Lopez, S., Reimers, D., D'Odorico, S., & Prochaska, J. X. 2002, A&A, 385, 778
- Lu, L., Sargent, W. L. W., & Barlow, T. A. 1998, AJ, 115, 55
- Ludwig, H.-G., Freytag, B., & Steffen, M. 1999, A&A, 346, 111
- Masana, E., Jordi, C., & Ribas, I. 2006, A&A, 450, 735
- Maeda, K., & Nomoto, K. 2003, ApJ, 598, 1163
- Meléndez, J., Shchukina, N.G., Vasiljeva, I.E., & Ramírez, I. 2006, ApJ, 642, 1082
- Molaro, P., Bonifacio, P., Centurión, M., et al. 2000, ApJ, 541, 54
- Nakamura, T., Umeda, H., Iwamoto, K.I., et al. 2001, ApJ, 555, 880
- Nissen, P.E. 1994, Rev. Mex. Astron. Astrofis. 29, 129
- Nissen, P.E., Chen, Y.Q., Asplund, M., & Pettini, M. 2004, A&A, 415, 993 (Paper I)
- Nissen, P.E., Gustafsson, B., Edvardsson, B., & Gilmore, G. 1994, A&A, 285, 440
- Nissen, P.E., Primas, F., Asplund, M., & Lambert, D.L. 2002, A&A, 390, 235
- Nissen, P.E., & Schuster, W.J. 1997, A&A, 326, 751
- Nomoto, K., Hashimoto, M., Tsujimoto, T. et al. 1997, Nucl. Phys. A, 616, 79
- Nomoto, K., Tominaga, N., Umeda, H., Kobayashi, C. & Maeda K. 2006, Nucl. Phys. A, 777, 424
- Norris, J.E., Ryan, S.G., & Beers T.C. 2001, ApJ, 561, 1034
- O'Brian, T.R., Wickliffe, M.E., Lawler, J.E., Whaling, W., & Brault, J.W. 1991, J. Opt. Soc. Am. B, 8, 1185
- Ohkubo, T., Umeda, H., Maeda, K., et al. 2006, ApJ, 645, 1352
- Petitjean, P., Srianand, R., & Ledoux, C. 2002, MNRAS, 332, 383
- Pettini, M., King, D. L., Smith, L. J., & Hunstead, R. W. 1997, ApJ, 478, 536
- Primas, F., Brugamyer, E., Sneden, C., et al. 2000, in: The First Stars, eds A. Weiss, T. Abel and V. Hill, ESO Astrophysics Ser., p. 51
- Prochaska, J. X., Howk, J. C., & Wolfe, A. M. 2003, Nature, 423, 57
- Prochaska, J. X., & Wolfe, A. M. 1999, ApJS, 121, 369
- Prochaska, J. X., & Wolfe, A. M. 2002, ApJ, 566, 68
- Prochaska, J. X., Wolfe, A. M., Howk, J. C., et al. 2007, ApJS, in press (astro-ph/0702325)
- Przybilla, N., & Butler, K. 2004, ApJ, 610, L61
- Ramaty, R., Scully, S.T., Lingenfelter, R.E., & Kozlovsky, B. 2000, ApJ, 534, 747
- Ramírez, I., Allende Prieto, C., Redfield, S., & Lambert, D.L. 2006, A&A, 459, 613
- Ramírez, I., & Meléndez, J. 2005a, ApJ, 626, 446
- Ramírez, I., & Meléndez, J. 2005b, ApJ, 626, 465
- Rix, S. A., Pettini, M., Steidel, C. C., et al. 2007, ApJ, submitted
- Ryan, S.G. 1989, AJ, 98, 1693
- Ryan, S.G., Norris, J.E., & Beers, T.C. 1999, ApJ, 523, 654
- Ryde, N. 2006, A&A, 455, L13
- Ryde, N., & Lambert, D.L. 2004, A&A, 415, 559
- Savage, B.D., & Mathis, J.S. 1979, ARA&A, 17, 73
- Schuster, W.J., Moitinho, A., Márquez, A., Parrao, L., & Covarrubias, E. 2006, A&A, 445, 939
- Schuster, W.J., & Nissen, P.E. 1988, A&AS, 73, 225
- Schuster, W.J., & Nissen, P.E. 1989, A&A, 221, 65
- Schuster, W.J., Nissen, P.E., Parrao, L., Beers, T.C., & Overgaard, L.P. 1996, A&AS, 117, 317
- Schuster, W.J., Parrao, L., & Contreras Martínez, M.E. 1993, A&AS, 97, 951
- Schnabel, R., Schultz-Johanning, M., & Kock, M. 2004, A&A, 414, 1169
- Skrutskie, M.F., Cutri, R.M., Stiening, R., et al. 2006, AJ, 131, 1163
- Stehlé, C., & Hutcheon, R. 1999, A&AS, 140, 93
- Steenbock, W., Holweger, H. 1984, A&A, 130, 319
- Takada-Hidai, M., Takeda, Y., Sato, S., et al. 2002, ApJ, 573, 614
- Takada-Hidai, M., Saito, Y., Takeda, Y., et al. 2005, PASJ, 57, 347
- Takeda, Y., Hashimoto, O., Taguchi, H., et al. 2005, PASJ, 57, 751
- Thielemann, F.-K., Nomoto, K., & Hashimoto, M. 1996, ApJ, 460, 408
- VandenBerg, D.A., Swenson, F.J., Rogers, F.J., Iglesias, C.A., & Alexander, D.R. 2000, ApJ, 532, 430
- Umeda, H., & Nomoto, K. 2003, Nature, 422, 871
- Umeda, H., & Nomoto, K. 2005, ApJ, 619, 427
- Vladilo, G., Centurión, M., Bonifacio, P., & Howk, J. C. 2001, ApJ, 557, 1007
- Wolfe, A.M., Gawiser, E., & Prochaska, J.X. 2005, ARA&A, 43, 861
- Woosley, S.E., & Weaver, T.A. 1995, ApJS, 101, 181

Appendix A: Line list and equivalent widths

Table A.1 gives a list of spectral lines used in this paper and the equivalent widths measured in the 2004 UVES spectra. Where no value is given, it is either because the line is too weak to provide a reliable abundance, or, in the case of the $\lambda\lambda 9212.9, 9237.5$ Si I lines, is affected by residuals from the removal of strong telluric H₂O lines. We also note that the Si I line at 9228.1 \AA is not included, because it falls close to the center of the Paschen-zeta line.

Appendix B: Photometric and spectroscopic indices

In Table B.1 the magnitudes V and K_s for our sample of stars are given together with the Strömgren indices ($b-y$), m_1 , c_1 and the photometric index of the H β line, $\beta(\text{phot})$. The table also gives the value of the $\beta(\text{UVES})$ index measured from the profile of H β in the UVES spectra. This index is defined as

$$\beta(\text{UVES}) = 10 \cdot \frac{F_{\text{Cb}} + F_{\text{Cr}}}{F_{\text{Lb}} + F_{\text{Lr}}}, \quad (\text{B.1})$$

where F_{Cb} , F_{Cr} are the fluxes in two 8 \AA wide pseudo-continuum bands centered $\pm 20 \text{ \AA}$ from the H β line center and F_{Lb} , F_{Lr} the fluxes in two 10 \AA wide line bands centered $\pm 7 \text{ \AA}$ from the center of H β . As seen from Fig. 3, the fluxes in the line bands are more affected by variations in effective temperature than the fluxes in the 'continuum' bands. Hence, the index becomes sensitive to T_{eff} .

Table A.1. List of spectral lines and equivalent widths measured in the UVES 2004 spectra of the following twelve stars: (1) CD $-24^{\circ}17504$, (2) CD $-71^{\circ}1234$, (3) CS 22943-095, (4) G 04-37, (5) G 48-29, (6) G 59-27, (7) G 126-52, (8) G 166-54, (9) HD 84937, (10) HD 338529, (11) LP 635-14, (12) LP 651-4.

ID	Wavelength Å	Exc.pot eV	loggf	Equivalent width													
				(1)	(2)	(3)	(4)	(5)	(6)	(7)	(8)	(9)	(10)	(11)	(12)		
Si I	8694.64	7.87	0.03										1.6				
Si I	9212.87	6.52	0.38	5.7	21.0	31.3	17.6	15.2	40.6	24.7	17.5	38.3	33.5	21.9	12.3		
Si I	9237.54	6.52	0.01		10.9	14.5	6.7	7.8	21.6		8.1	16.9	15.5	9.0			
Fe I	4199.10	3.05	0.16	10.3	36.9	41.8	34.7	23.4	55.2	41.3	26.2	46.9	42.1	36.3	25.4		
Fe I	4233.60	2.48	-0.58	6.5	28.4	33.2	26.1	14.4	49.4	32.9	18.2	38.7	33.0	26.6	17.2		
Fe I	4250.12	2.47	-0.38	9.8	37.8	42.6	34.4	22.4	58.7	42.2	25.3	48.3	43.2	36.3	24.9		
Fe I	4271.15	2.45	-0.34	11.5	41.3	45.6	39.0	26.0	63.6	46.0	28.8	52.7	46.6	39.6	26.9		
Fe I	4282.40	2.18	-0.78	7.5	30.2	35.7	27.9	17.7	51.7	35.3	20.1	41.5	35.7	29.4	18.4		
Fe I	4918.99	2.86	-0.34	5.5	25.3	29.9	22.8	13.0	45.9	30.1	15.4	35.1	30.0	24.0	14.9		
Fe I	4920.50	2.83	0.07	12.8	44.6	49.7	42.4	28.9	66.9	50.5	31.5	56.1	50.3	43.0	31.2		
Fe II	4178.86	2.58	-2.61	1.9	11.2	14.6	9.0	6.6	25.7	14.5	7.9	19.9	15.8	11.5	6.1		
Fe II	4233.17	2.58	-2.01	6.0	32.3	37.6	28.4	20.1	51.5	39.0	19.9	45.8	40.1	33.0	19.4		
Fe II	4416.83	2.78	-2.65		7.1	9.4	6.0	4.2	16.8	9.7	4.5	13.4	10.0	7.7	4.3		
Fe II	4489.18	2.83	-2.96		3.3	4.6	3.0		9.1	4.7	2.1		4.8	3.2	1.5		
Fe II	4491.41	2.85	-2.80		4.3	6.1	3.6	2.4	11.2	6.3	2.8	8.6	6.3	4.9	2.9		
Fe II	4508.29	2.85	-2.41		11.1	13.8	9.2	5.4	23.7	13.9	6.7	18.6	15.0	9.7	6.2		
Fe II	4515.34	2.84	-2.56		7.7	10.3	6.7	5.3	18.2	11.2	4.8	14.1	11.7	7.7	4.6		
Fe II	4520.23	2.81	-2.66		7.4	9.7	5.8	3.8	16.2	9.6	4.2	12.3	10.1	7.3	3.6		
Fe II	4522.63	2.84	-2.22	2.4	16.1	19.8	12.6	9.0	32.6	21.1	9.0	26.7	21.4	16.3	8.7		
Fe II	4541.52	2.85	-3.04		3.4	3.7			7.2	3.7	1.5	5.6	4.6	2.7	1.5		
Fe II	4555.89	2.83	-2.43		10.4	13.6	9.2	6.2	23.4	14.8	5.5	18.6	15.0	11.0			
Fe II	4576.34	2.84	-3.01		3.4	4.0	1.9		7.3	4.1	1.7	5.7	4.5	2.6	3.0		
Fe II	4583.84	2.81	-1.91	4.9	27.8	33.4	23.8	17.8	47.5	34.3	17.5	41.5	35.9	29.0	17.2		
Fe II	4923.93	2.89	-1.45	12.2	46.9	52.4	42.5	33.4	67.5	54.8	33.2	61.9	56.0	47.8	33.7		
Zn I	4722.15	4.03	-0.39	0.9	2.8	2.8	2.0	1.2	5.9	3.1	1.1	3.3	3.2	2.4	0.9		
Zn I	4810.53	4.08	-0.17	1.4	3.0	4.9	3.1	1.7	7.5	4.2	1.9	5.5	4.3	3.3	2.0		

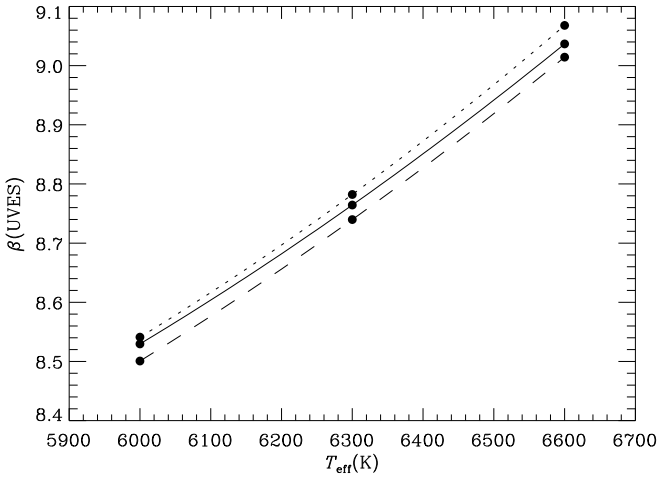


Fig. B.1. The relation between $\beta(\text{UVES})$ and T_{eff} as calculated for a set of model atmospheres. The full drawn line corresponds to $\log g = 4.3$, $[\text{Fe}/\text{H}] = -2.0$, the dotted line to $\log g = 3.9$, $[\text{Fe}/\text{H}] = -2.0$, and the dashed line to $\log g = 4.3$, $[\text{Fe}/\text{H}] = -3.2$.

T_{eff} was derived from the observed value of $\beta(\text{UVES})$ by quadratic interpolation between theoretical $\beta(\text{UVES})$ values calculated for a grid of 105 model atmospheres with $T_{\text{eff}} = 5400, 5700, 6000, 6300, 6600$ K, $\log g = 3.5, 3.9, 4.3$, and $[\text{Fe}/\text{H}] = -0.8, -1.2, -1.6, -2.0, -2.4, -2.8, -3.2$.

In Fig. B.1 some of the calculated $\beta(\text{UVES})$ values are plotted as a function of T_{eff} together with the interpolation lines. As seen, the variation of $\beta(\text{UVES})$ with $\log g$ and $[\text{Fe}/\text{H}]$ is small compared to the change of $\beta(\text{UVES})$ as a function of T_{eff} . For an observational error ± 0.015 of $\beta(\text{UVES})$ and errors ± 0.15 dex of $\log g$ and $[\text{Fe}/\text{H}]$, T_{eff} is determined to a precision of about ± 20 K.

As seen from Fig. B.2 there is a good correlation between $\beta(\text{phot})$ and $\beta(\text{UVES})$. A maximum likelihood fit that takes into account the estimated errors of the two indices gives the following relation:

$$\beta(\text{phot}) = 1.474 + 0.129 \cdot \beta(\text{UVES}) \quad (\text{B.2})$$

with a reduced χ^2 close to one. The dominant contribution to the scatter in Fig. B.2 comes from the error of $\beta(\text{phot})$. According to Eq. (B.2), the error of $\beta(\text{UVES})$ (± 0.015) corresponds to an error of ± 0.002 in $\beta(\text{phot})$, which is a factor of three lower than the actual error of the $\beta(\text{phot})$ observations (Schuster & Nissen 1988). Hence, we have used Eq. (B.2) to predict an improved $\beta(\text{phot})$ value of our stars before calculating the interstellar reddening excess from the $(b-y)_0$ calibration equations of Schuster & Nissen (1989) with a zero point shift of 0.005 mag. added (Nissen 1994). The so derived value of $E(b-y)$ is given in column 10 of Table B.1.

From this discussion it also follows that the error of T_{eff} determined from the photometric $H\beta$ index would be three times higher than the error of T_{eff} determined from $\beta(\text{UVES})$. On the other hand, it is seen from Fig. B.3 that

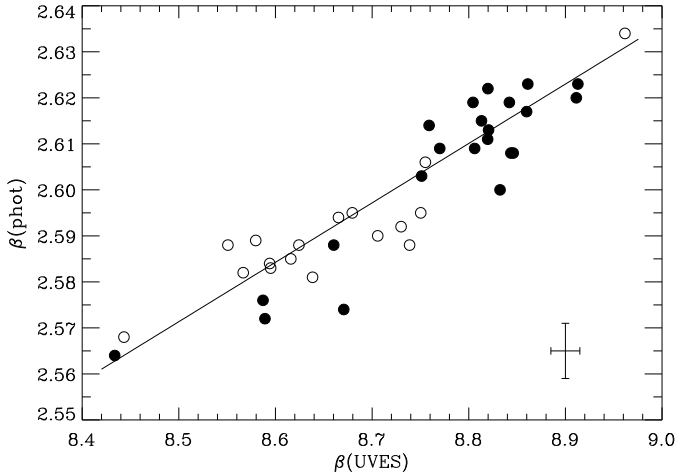


Fig. B.2. The photometric index of the $H\beta$ line vs. the index measured from the profile of $H\beta$ in UVES spectra. $1-\sigma$ error bars: $\sigma(\beta(\text{UVES})) = \pm 0.015$ and $\sigma(\beta(\text{phot})) = \pm 0.006$ are shown in the lower right corner. Stars having $[\text{Fe}/\text{H}] < -2.0$ are plotted with filled circles, and stars having $-2.0 < [\text{Fe}/\text{H}] < -1.0$ with open circles.

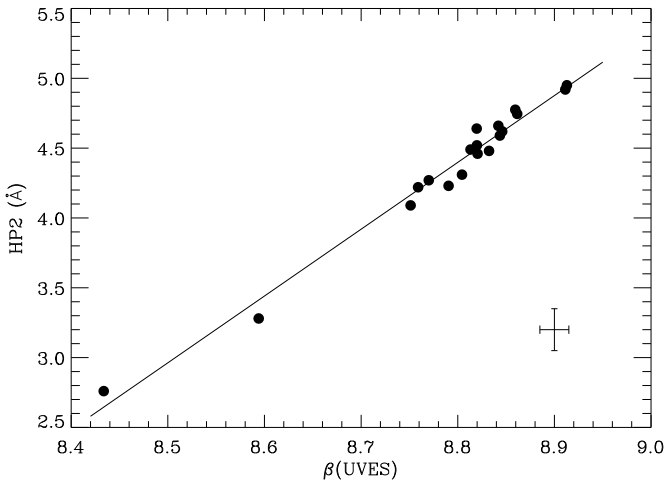


Fig. B.3. The HP2 index of the $H\delta$ line (from Ryan et al. 1999) vs. $\beta(\text{UVES})$.

the HP2 index of the $H\delta$ line (Beers et al. 1999) correlates extremely well with $\beta(\text{UVES})$ for 19 stars in common with Ryan et al. (1999). Hence, for the group of metal-poor turnoff stars, one may use the HP2 index, which is based on medium-resolution spectra, to determine differential values of T_{eff} with the same high precision as obtained from $\beta(\text{UVES})$.

The absolute visual magnitude of a star, $M_V(\text{phot})$, is determined from the Strömgren indices ($b-y$), m_1 , c_1 using a calibration derived by Schuster et al. (2006) for a sample of stars with accurate ($\sigma(\pi)/\pi < 0.15$) Hipparcos parallaxes. Reddening corrections were applied if $E(b-y) > 0$. The derived values of $M_V(\text{phot})$ are given in column 11 of Table B.1. In columns 12 and 13, the absolute magnitude derived directly from the Hipparcos parallax and its error are given for stars with a parallax error less than 30%.

Appendix C: S and Zn abundances in DLAs

Table C.1 provides a compilation of S and Zn abundances in 20 DLA systems as derived from high-resolution spectra obtained with 8-10 m class telescopes. References to the original works are given in the last column of the Table. S abundances have been determined from the $\lambda\lambda 1250, 1253, 1259$ S II triplet and Zn abundances from the $\lambda\lambda 2026, 2062$ Zn II doublet. Both S II and Zn II are the major ionization stages of their respective elements in H I regions, and corrections for unobserved ion stages are expected to be unimportant (e.g. Vladilo et al. 2001). Neither S nor Zn show much affinity for dust and the problem is further lessened in DLAs which generally show only mild depletions of even the refractory elements (Pettini et al. 1997). Hence, the values given in Table C.1 should reflect the true interstellar abundances of these two elements in the high redshift galaxies giving rise to the damped Lyman-alpha systems.

Table B.1. V and K_s magnitudes, Strömrgren indices, and photometric and spectroscopic indices of the strength of the H β line. The derived interstellar reddening of $(b-y)$ is given in column 10, and the absolute visual magnitude derived from the Strömrgren photometry is given in col. 11. Columns 12 and 13 give the absolute visual magnitude and its 1- σ error derived from the Hipparcos parallax if available with an error less than 30%.

ID	V	K_s	$b-y$	m_1	c_1	$\beta(\text{phot})$	Ref. ^{a)}	$\beta(\text{UVES})$	$E(b-y)$	$M_V(\text{phot})$	$M_V(\text{par})$	σ
BD -13°3442	10.288	9.018	0.308	0.050	0.385	2.622	4	8.820	0.022	3.67		
CD -30°18140	9.949	8.655	0.323	0.047	0.344	2.606	1	8.755	0.019	3.88	4.19	0.46
CD -35°14849	10.568	9.293	0.321	0.040	0.293	2.603	1	8.751	0.011	4.47		
CD -42°14278	10.216	8.770	0.361	0.040	0.229	2.576	1	8.587	0.015	4.94		
G 11-44	11.091	9.740	0.335	0.061	0.248	2.588	1	8.660	-0.005	4.80		
G 13-09	9.998	8.739	0.311	0.048	0.373	2.609	1	8.806	0.021	3.75	3.70	0.59
G 18-39	10.392	9.017	0.346	0.073	0.286	2.581	1	8.638	0.002	4.35		
G 20-08	9.948	8.498	0.356	0.047	0.251	2.574	1	8.671	0.020	4.79	4.47	0.43
G 24-03	10.467	9.020	0.363	0.057	0.271	2.585	1	8.616	0.019	4.53		
G 29-23	10.230	8.831	0.339	0.059	0.332	2.590	1	8.706	0.017	3.87		
G 53-41	11.022	9.595	0.356	0.083	0.271	2.589	1	8.580	-0.003	4.54		
G 64-12	11.459	10.208	0.307	0.043	0.337	2.617	4	8.860	0.020	4.37		
G 64-37	11.144	9.923	0.300	0.054	0.333	2.623	4	8.861	0.007	4.31		
G 66-30	11.028	9.789	0.305	0.072	0.358	2.634	1	8.962	0.016	4.20		
G 126-62	9.478	8.075	0.330	0.063	0.327	2.588	1	8.739	0.012	4.00	4.06	0.37
G 186-26	10.829	9.590	0.306	0.041	0.339	2.608	1	8.844	0.019	4.31	5.12	0.50
HD 106038	10.179	8.761	0.342	0.092	0.264	2.583	1	8.595	-0.017	4.69	4.99	0.36
HD 108177	9.671	8.354	0.330	0.059	0.287	2.594	1	8.665	-0.002	4.36	4.87	0.26
HD 110621	9.906	8.566	0.337	0.067	0.324	2.595	1	8.679	0.007	3.89	4.12	0.46
HD 140283	7.213	5.588	0.380	0.033	0.284	2.564	1	8.434	0.013	3.83	3.36	0.12
HD 160617	8.733	7.311	0.347	0.051	0.331	2.584	1	8.594	0.010	3.51	3.37	0.31
HD 179626	9.210	7.680	0.373	0.095	0.293	2.588	1	8.551	0.005	4.29	3.57	0.39
HD 181743	9.687	8.274	0.351	0.052	0.224	2.582	1	8.567	-0.001	4.97	4.95	0.34
HD 188031	10.148	8.857	0.328	0.058	0.310	2.592	1	8.730	0.009	4.19		
HD 193901	8.660	7.144	0.383	0.099	0.221	2.568	1	8.443	-0.006	5.16	5.46	0.12
HD 194598	8.354	6.982	0.344	0.091	0.269	2.588	1	8.624	-0.011	4.63	4.62	0.15
HD 215801	10.044	8.642	0.334	0.049	0.330	2.572	1	8.589	-0.001	3.47		
LP 815-43	10.912	9.650	0.304	0.048	0.382	2.623	1	8.913	0.031	4.18		
CD -24°17504	12.124	10.807	0.322	0.043	0.283	2.609	4	8.770	0.010	4.60		
CD -71°1234	10.44	9.114					5	8.790	0.019	3.67		
CS 22943-095	11.762	10.469	0.324	0.045	0.335	2.619	3	8.804	0.025	4.17		
G 04-37	11.426	9.974	0.363	0.031	0.306	2.614	4	8.759	0.053	4.43		
G 48-29	10.467	9.264	0.298	0.057	0.351	2.620	4	8.911	0.013	4.29		
G 59-27	10.892	9.560	0.321	0.058	0.301	2.595	1	8.750	0.004	4.32		
G 126-52	10.996	9.719	0.322	0.045	0.347	2.608	2	8.846	0.031	4.20		
G 166-54	11.005	9.731	0.324	0.043	0.322	2.619	4	8.842	0.027	4.42		
HD 84937	8.332	7.062	0.303	0.056	0.354	2.613	1	8.821	0.009	3.95	3.77	0.19
HD 338529	9.370	8.144	0.308	0.045	0.366	2.600	1	8.832	0.023	3.98	3.48	0.46
LP 635-14	11.362	9.997	0.347	0.026	0.366	2.611	4	8.820	0.060	4.02		
LP 651-4	12.053	10.842	0.321	0.023	0.340	2.615	4	8.813	0.033	4.27		

^{a)} References of V , $b-y$, m_1 , c_1 and $\beta(\text{phot})$: (1) Schuster & Nissen (1988), (2) Schuster et al. (1993), (3) Schuster et al. (1996), (4) Schuster et al. (2006), (5) Ryan (1989). For all stars, K_s has been taken from the 2MASS catalogue (Skrutski et al. 2006).

Table C.1. S and Zn abundance measurements in DLAs

QSO	z_{abs}	$\log N(\text{H I})$ (cm^{-2})	$\log N(\text{S II})$ (cm^{-2})	$\log N(\text{Zn II})$ (cm^{-2})	$[\text{Zn}/\text{H}]^{\text{a}}$	$[\text{S}/\text{Zn}]^{\text{b}}$	Ref. ^c
Q0000–2620	3.3901	21.41 ± 0.08	14.70 ± 0.03	12.01 ± 0.05	–2.01	+0.14	10
Q0013–004	1.97296	20.83 ± 0.05	15.28 ± 0.03	12.74 ± 0.04	–0.70	–0.01	11
Q0100+130	2.30903	21.37 ± 0.08	15.09 ± 0.06	12.47 ± 0.01	–1.51	+0.07	2
Q0201+365	2.4628	20.38	15.29 ± 0.01	12.76 ± 0.05	–0.23	–0.02	14, 12
Q0407–4410	2.5505	21.13 ± 0.10	14.82 ± 0.06	12.44 ± 0.05	–1.30	–0.17	8
Q0407–4410	2.5950	21.09 ± 0.10	15.19 ± 0.05	12.68 ± 0.02	–1.02	–0.04	8
B0528–250	2.8120	21.11 ± 0.04	15.56 ± 0.02	13.27 ± 0.03	–0.45	–0.26	1
Q0551–366	1.96221	20.50 ± 0.08	15.38 ± 0.11	13.02 ± 0.05	–0.09	–0.19	6
FJ081240.6+320808	2.6263	21.35	15.63 ± 0.08	13.15 ± 0.02	–0.81	–0.07	13
0841+1256	2.37452	20.99 ± 0.08	14.69 ± 0.05	12.10 ± 0.02	–1.50	+0.04	3
0841+1256	2.47621	20.78 ± 0.08	14.48 ± 0.10	11.69 ± 0.10	–1.70	+0.24	3
SDSS1116+4118A	2.9422	20.28 ± 0.05	15.01 ± 0.10	12.40 ± 0.33	–0.49	+0.06	5
LBQS 1210+1731	1.89177	20.63 ± 0.08	14.96 ± 0.02	12.40 ± 0.05	–0.84	+0.01	3
Q1331+170	1.77637	21.14 ± 0.08	15.08 ± 0.11	12.54 ± 0.02	–1.21	–0.01	2
HE2243–6031	2.33000	20.67 ± 0.02	14.88 ± 0.01	12.22 ± 0.03	–1.06	+0.11	7
B2314–409	1.8573	20.90 ± 0.10	15.10 ± 0.05	12.52 ± 0.03	–0.99	+0.03	4
LBQS 2230+0232	1.86359	20.83 ± 0.05	15.29 ± 0.06	12.72 ± 0.05	–0.72	+0.02	3
Q2231–002	2.06616	20.53 ± 0.08	15.10 ± 0.15	12.30 ± 0.05	–0.84	+0.25	2
Q2343+125	2.4313	20.35 ± 0.05	14.71 ± 0.08	12.45 ± 0.06	–0.51	–0.29	9
Q2343–BX415	2.5739	20.98 ± 0.05	15.38 ± 0.03	12.90 ± 0.06	–0.69	–0.07	15

^a $[\log (\text{Zn}/\text{H})_{\text{DLA}} - \log (\text{Zn}/\text{H})_{\odot}]$, where $\log (\text{Zn}/\text{H})_{\odot} = -7.39$ (Asplund et al. 2005).

^b $[\log (\text{S}/\text{Zn})_{\text{DLA}} - \log (\text{S}/\text{Zn})_{\odot}]$, where $\log (\text{S}/\text{Zn})_{\odot} = 2.55$ (Asplund et al. 2005).

^c References— 1: Centúron et al. (2003); 2: Dessauges-Zavadsky et al. (2004); 3: Dessauges-Zavadsky et al. (2006,2007); 4: Ellison & Lopez (2001); 5: Ellison et al. (2001); 6: Ledoux et al. (2002); 7: Lopez et al. (2002); 8: Lopez & Ellison (2003); 9: Lu et al. (1998); 10: Molaro et al. (2000); 11: Petitjean et al. (2002); 12: Prochaska et al. (2007); 13: Prochaska et al. (2003); 14: Prochaska & Wolfe (1999); 15: Rix et al. (2007).